

# Mesospheric HO<sub>x</sub> chemistry from microwave observations of H<sub>2</sub>O<sub>2</sub>, O<sub>3</sub>, and H<sub>2</sub>O

Brad J. Sandor,<sup>1</sup> R. Clancy,<sup>2</sup>

Received ; revised ; accepted

Short title: MESOSPHERIC HO<sub>2</sub> OBSERVATIONS

<sup>1</sup>Jet Propulsion Laboratory, California Institute of Technology, Pasadena.

<sup>2</sup>Space Science Institute, 110111 (131), Colorado.

## Abstract.

Microwave ( $\lambda \sim 1.72$  mm) spectral emission line observations of HO<sub>2</sub>, O<sub>3</sub>, and H<sub>2</sub><sup>18</sup>O from the upper stratosphere and mesosphere (45-80 km) were obtained in April 1992, January 1993, April and December 1996, using the Kitt Peak National Radio Astronomy Observatory (NRAO). Significant improvements to this, the only method for making mesospheric HO<sub>2</sub> measurements, have been made with hardware upgrades allowing observation of a stronger emission line than described in previous work. Data analysis has been improved by (1) recalibration of the (primarily astronomical) instrument for atmospheric studies, (2) incorporation of updated laboratory spectroscopic work, and (3) use of an improved photochemical model. Diurnal HO<sub>2</sub> data analyses employing 30 minute to 2 hour observations show measured HO<sub>2</sub> abundances at 50-80 km altitude are 23-47% higher than photochemical model values at mid-day, agree with model values prior to 9am, and exceed model mixing ratios by 100% immediately after sunset. Coordinated diurnal measurements of mesospheric O<sub>3</sub> find a model O<sub>3</sub> deficit consistent with model underprediction of ozone seen in all comparable data sets. The ozone model deficit and 9am-6pm HO<sub>2</sub> model deficit are simultaneously resolved with a 40% reduction in the rate coefficient  $k(\text{HO}_2 + \text{O} \rightarrow \text{O}_3 + \text{H})$ . We briefly review other modeling studies of this rate change, indicating it has negligible effect in the lower stratosphere and improves a diverse set of model results from the stratosphere to mesopause. We argue that the factor of two model underprediction of post-sunset HO<sub>2</sub> is driven by rapid conversion of O to O<sub>3</sub> in the absence of photolysis, and resultant conversion of H to HO<sub>2</sub> in the 70-80 km altitude range.

## 1. Introduction

The HO<sub>x</sub> family (HO<sub>2</sub>, OH, and H) contributes to ozone loss processes throughout the atmosphere via catalytic O<sub>x</sub> (O<sub>3</sub> and O) destruction, and completely dominates O<sub>x</sub> loss above 55 km [e.g. Braeser and Solomon, 1986]. Despite the importance of these odd-hydrogen species in the mesosphere, their abundances there are poorly constrained by measurements. Balloon measurements in the low to mid-stratosphere [Traub et al., 1990; Stimpfle et al., 1990; Park and Carli, 1991; Stachnik et al., 1992] find [HO<sub>2</sub>] values in agreement with photochemical model predictions up to 40 km altitude, but the highest (upper stratospheric) balloon measurements [Traub et al., 1990; Stachnik et al., 1992] find models underpredict [HO<sub>2</sub>] by about 30% at 40-50 km.

The first mesospheric measurements of HO<sub>2</sub> were made using ground-based microwave spectroscopy by Clancy et al. [1994a], who found a large excess of measured HO<sub>2</sub> relative to photochemical model abundances at 50-75 km. Model underprediction of mesospheric [HO<sub>2</sub>] is a surprising result in the context of model underprediction of ozone (the long-standing ozone deficit problem, which has been reduced by roughly one half through changes in the rate coefficient for OH + HO<sub>2</sub> → O<sub>2</sub> + H<sub>2</sub>O) [Solomon et al., 1983; Clancy et al., 1987; Fluszkiewicz and Allen, 1993]. Most changes to the photochemical model that reduce the HO<sub>2</sub> deficit increase ozone destruction and worsen the model O<sub>3</sub> deficit. Clancy et al. [1994a] showed that a decrease in the accepted JPL92 rate coefficient for O + HO<sub>2</sub> → OH + O<sub>2</sub> would simultaneously reduce both the HO<sub>2</sub> and O<sub>3</sub> deficits. Another consequence of decreasing the rate of this HO<sub>x</sub> partitioning reaction is a decrease in OH abundance below that predicted with the standard photochemical model.

Subsequent mesospheric [OH] measurements [Summers et al., 1996; 1997; Conway et al., 1996] indeed found 30 to 50% model overprediction of [OH] at altitudes 50-70 km, an OH model surplus that Summers et al. [1996; 1997] show is resolved by a 50% reduction in the O + HO<sub>2</sub> → OH + O<sub>2</sub> rate coefficient. As for the case of HO<sub>2</sub>, OH

measurements below 40 km [eg Pickett and Peterson, 1996] are in general agreement with model prediction.

The implications of a reduced  $k(\text{O} + \text{HO}_2)$  rate coefficient on aspects of atmospheric chemistry other than mesospheric  $\text{HO}_2$ ,  $\text{O}^1\Delta_g$ , and  $\text{O}_3$  are generally consistent with, and supportive of this change. Sandor et al. [1997] used the rate change to resolve a lower mesospheric  $\text{O}_2(^1\Delta_g)$  model deficit that parallels the  $\text{O}_3$  deficit. In a study of exothermic chemistry, Siskind et al. [1996] found a reduced value for  $k(\text{O} + \text{HO}_2)$  alleviates a model cold bias in the upper mesosphere. Model underprediction of column CO above 64 km is described by Solomon et al. [1985], who discuss a model overestimate of OH abundance as one possible reason for the CO underestimate. Khosravi et al. [1997] show that 40% reduction of the  $\text{O} + \text{HO}_2$  rate coefficient, in coordination with assimilation of Upper Atmospheric Research Satellite (UARS)  $\text{ClO}_x$  and  $\text{NO}_x$  data and UKMO temperature data, eliminates the ozone deficit in the upper stratosphere. The  $\text{O} + \text{HO}_2$  reaction is unimportant in the lower stratosphere, where both  $\text{HO}_2$  and atomic oxygen abundances are very low. Chin et al. [1997] show, for example, that  $\text{HO}_2$  is responsible for less than 1% of lower stratospheric  $\text{O}_3$  destruction. Summers et al. [1997] find that a 50% reduction of the  $\text{O} + \text{HO}_2$  rate coefficient implies changes of less than 10% to  $\text{O}^1\Delta_g$  and  $\text{HO}_2$  abundances below 30 km.

Since the Clancy et al. [1994a] result, hardware improvements have allowed observations of a stronger  $\text{HO}_2$  emission line, resulting in new data with improved s/n. Observations of the 233.9 GHz  $^{18}\text{O}^{16}\text{O}$  line [Sandor and Clancy, 1997] have been used to improve calibration of the Clancy et al. [1994a] measurement system. In work presented below the effect of this new calibration, together with use of an improved photochemical model [Siskind et al., 1995] and application to a larger  $\text{HO}_2$  data set, leads to corroboration of the Clancy et al. [1994a] conclusion. From mid-day high signal to noise (s/n) observations on six dates, we measure  $\text{HO}_2$  abundances 23% to 47% higher than model prediction for altitudes 50-80 km. Model agreement with the data is substantially im-

proved for a 40% (two sigma) reduction of  $k(\text{O}(\text{I}) + \text{HO}_2)$  below the accepted 1991 value [DeMore *et al.*, 1991, henceforward referenced as J1 '1991. This rate is unchanged from the 1992 value].

## 2. HO<sub>2</sub> Photochemistry and Photochemical Modeling

HO<sub>2</sub>, OH, and H are rapidly interconverted during HO<sub>x</sub> catalytic ozone destruction cycles. For 50-70 km altitude, HO<sub>2</sub>, OH, and H individually have chemical lifetimes  $\leq 10$  seconds, while the lifetime of HO<sub>x</sub> is about an hour. Above 70 km, HO<sub>2</sub> and OH lifetimes become shorter while the HO<sub>x</sub> lifetime increases to one day at 80 km [Brasseur and Solomon, 1986]. HO<sub>x</sub> production for these altitudes is dominated by Schumann-Runge Band photolysis and O(<sup>1</sup>D) oxidation of water:



HO<sub>x</sub> removal proceeds via reactions among HO<sub>x</sub> species. Below 75 km, the important HO<sub>x</sub> destruction reaction is:



with atomic hydrogen playing a more important role at higher altitudes.

HO<sub>x</sub> partitioning reactions, which interchange H, OH and HO<sub>2</sub> without changing the total of their concentrations, determine the ratio  $[\text{H}]/[\text{OH}]$ . For 50-80 km the important partitioning reactions are R5, R6, R7, and R11 (table 1). From these one can write algebraic expressions for the photochemical equilibrium concentrations of the HO<sub>x</sub> species and solve for the HO<sub>2</sub>/OH ratio:

$$\frac{d[\text{HO}_2]}{dt} = k_5 k_7 \frac{[\text{O}_2][\text{M}]}{k_6 k_7 [\text{O}_2] + k_{11} [\text{O}_3]} \quad (1)$$

As part of the data interpretation a one dimensional photochemical model [Siskind *et al.*, 1995] was used to calculate theoretical abundances of chemical species as a function of time of day. This model, an updated version of that used by Rusch and Eckman [1985] and by Clancy *et al.* [1994a], calculates species abundances at 2 km intervals for altitudes of 36-82 km. Species with photochemical lifetimes sufficiently long that horizontal transport is important are specified as model inputs. The key long-lived species for this study is water, for which the input profile is derived from the 203 GHz  $\text{H}_2^{18}\text{O}$  observations. We use  $\text{H}_2^{18}\text{O}$  as a proxy for the normal isotope,  $\text{H}_2^{16}\text{O}$ , based upon observations showing the ratio  $[\text{H}_2^{18}\text{O}]/[\text{H}_2^{16}\text{O}]$  in the atmosphere is constant within a range less than  $\pm 2\%$  [Kaye, 1987]. Model  $\text{HO}_2$  and  $\text{O}_3$  abundances scale as  $[\text{H}_2\text{O}]^{1/2}$  and  $[\text{H}_2\text{O}]^{-1/2}$ , respectively [Clancy *et al.*, 1994a], so a (typical)  $\pm 20\%$  uncertainty in measured water vapor corresponds to  $\pm 10\%$  uncertainties in model  $\text{HO}_2$  and ozone. It is significant that an error in water vapor input to the model produces errors in model  $\text{HO}_2$  and  $\text{O}_3$  that are opposite in sign, because this means an error in measured water vapor cannot cause the observed simultaneous underpredictions of  $\text{HO}_2$  and  $\text{O}_3$ .

The standard version of the Siskind *et al.* [1995] model includes some 50 photochemical reactions. Reactions relevant to mesospheric  $\text{HO}_x$  chemistry are listed in Table 1. The standard model was run with 111,4 reaction rates. Altered versions of the standard model were run by perturbing reaction rates relative to 111,91 values. The modified model version of most interest differs from the standard model in that it uses a rate coefficient for  $\text{HO}_2 + \text{O} \rightarrow \text{OH} + \text{O}_2$  reduced 40% (twice the quoted uncertainty) below the standard 111,94 value. The focus on this reaction follows from Clancy *et al.* [1994a], where the 40% magnitude of the perturbation is determined from  $\text{HO}_2$  observations described in the present work.

### 3. Observations and Data Analysis

Observations of HO<sub>2</sub> at 254.55153 and 260.56586 GHz, O<sub>3</sub> at 249.7886 GHz, and H<sub>2</sub><sup>18</sup>O at 203.40752 GHz were made from Kitt Peak Arizona (32°N, 112°W), using the National Radio Astronomy Observatory (NRAO)<sup>3</sup> 12-meter radio telescope and microwave receivers. HO<sub>2</sub> observations were made at 255 GHz prior to 01 December 1995, and at 260 GHz subsequently. The 260.6 GHz HO<sub>2</sub> line is preferred because it is 58% stronger than the 254.6 GHz line [Pickett *et al.*, 1996]. The weaker line was used for earlier observations owing to problems with tuning the receivers to the higher frequency, which is closer to the putative edge of the 200-265 GHz receiver sensitivity. Experience has led to the capability of tuning with confidence to 260.6 GHz, with noise comparable to that at 254.6 GHz. [H<sub>2</sub><sup>18</sup>O] is measured as a proxy for [H<sub>2</sub>O], which is used as an input to the photochemical model. [O<sub>3</sub>] measurements are important for understanding the relationship between HO<sub>x</sub> and ox chemistry discussed in the preceding section.

Observations are made with the telescope at 20° or 30° elevation and fixed azimuth. Species abundances are roughly linearly proportional to spectral brightness temperatures for these optically thin emissions, and the corresponding rotational states are in local thermodynamic equilibrium well into the thermosphere. Line strengths, as well as line center frequencies and rotational state energy levels are taken from the JPL microwave spectroscopy catalog [Poynter and Pickett, 1985; Pickett *et al.*, 1996]. Line shapes follow a Voigt profile dominated by collisional (pressure) broadening up to altitudes of about 65 km. Thermal (Doppler) broadening becomes important above 65 km, and dominates the line shape above 75 km. The exponential dependence of pressure on altitude allows derivation of species altitude dependence from line shape for altitudes where collisional broadening is important. A frequency switching procedure is used to remove the base-

---

<sup>3</sup>The National Radio Astronomy Observatory is operated by Associated Universities, Inc., under cooperative agreement with the National Science Foundation.

line, making the observations insensitive to (very broad) emission from below about 45 km. Species abundances are retrieved from spectral data using an iterative least squares inversion to minimize the summed squared residuals between the data and a synthetic spectrum corresponding to the retrieved species altitude profile. More detailed discussions of microwave radiative transfer, frequency switching, and least squares inversions are provided in *Clancy and Muhleman* [1993] and *Clancy et al.* [1994a]. Retrievals require an assumed temperature profile, which we adapt from the CIRA 86 [*Fleming et al.*, 1990] and expanded Solar Mesospheric Explorer (SME) [*Clancy et al.*, 1994b] climatologies, and from which we calculate hydrostatic equilibrium pressures. Reasonable deviations from climatological temperatures lead to 0% to 2% retrieval errors.

Subsequent to *Clancy et al.* [1994a], improvements to the microwave data analysis have been made by recalibrating the Kitt Peak observations [*Sandor and Clancy*, 1997], and by incorporating recent laboratory measurements of HO<sub>2</sub> spectroscopic parameters [*Chance et al.*, 1995; 1997]. The need for a recalibration follows from the atmosphere filling  $2\pi$  steradians of sky, while standard Kitt Peak calibration procedures are designed for observations of small angular size astronomical objects. The result of the recalibration is that 20° elevation observations have their brightness temperatures revised downward by 16%. While this reduces retrieved [HO<sub>2</sub>] by 16%, it also reduces retrieved [H<sub>2</sub><sup>18</sup>O] (used as a proxy for H<sub>2</sub>O [*Clancy et al.*, 1994a]) by 16%, thereby decreasing the measured water abundance used as an input to the photochemical model. Since model [HO<sub>2</sub>] scales as [H<sub>2</sub>O]<sup>1/2</sup>, the new calibration reduces model underprediction of [HO<sub>2</sub>] by only ~8%.

For HO<sub>2</sub>, hyperfine splitting of the 254 and 260 GHz HO<sub>2</sub> lines by 240 and 440 KHz, respectively, and updated line strengths [*K. Chance, personal communication*, 1997] have been incorporated in the data reduction procedure. Updated strengths for the four hyperfine components amount to a 3.9% decrease for the 254 GHz line and a 3.2% increase for the 260 GHz line relative to the JPL catalog values.

The pressure broadening coefficient ( $V_{co}$ ) for these HO<sub>2</sub> lines remains unmeasured.

*de Zafra et al. [1984]* estimated  $V_{co} = 3.1 \pm 0.6$  MHz/hPa for their stratospheric observations of HO<sub>2</sub> lines at 265.690, 265.732, and 265.770 GHz, basing that estimate on an approximately linear relationship between dipole strength and  $V_{co}$  for a number of other molecules with well known microwave and infrared pressure broadening behaviors. *Nelson and Zahniser [1994]* measured  $V_{co} = 3.2040.27$  MHz/hPa for an  $\nu_2$  line in the  $\nu_2$  vibrational band corresponding to the pure rotational line at 578.196 GHz. *Chance et al. [1994]* measured  $V_{co} = 4.16 \pm 0.38$  MHz/hPa for the HO<sub>2</sub> line at 2.4878 THz. We interpret the *Nelson and Zahniser [1994]* measurement as verification of the *de Zafra et al. [1984]* estimate, and the *Chance et al. [1994]* measurement as indicating  $V_{co}$  increases with transition frequency. Based on these measurements, we continue to use the *de Zafra et al. [1984]* value, but with reduced uncertainty,  $V_{co} = 3.1 \pm 0.3$  MHz/hPa. 10% uncertainty in the pressure broadening coefficient corresponds to 0-8% uncertainties in the retrieved mixing ratios.

Spectral data for the 260 and 254 GHz HO<sub>2</sub> lines are shown in figures 1 and 2, respectively. Contribution functions (figure 3) corresponding to the (figure 1) 260 GHz spectrum are indicative of altitude resolution of the retrieval. Minimum half-widths are 10-15 km, delimiting the the best possible altitude resolution. Contribution functions indicate the relative contributions of HO<sub>2</sub> at different altitudes to the observed spectrum, and correspond to the weighting functions [*Clancy et al., 1994a*] multiplied by the HO<sub>2</sub> mixing ratios. Figure 3 indicates most of the information content of an HO<sub>2</sub> spectrum derives from emission near 70 km altitude. Retrieved HO<sub>2</sub> abundance at any altitude is well approximated by [*Rodgers, 1990*]:

$$\mathbf{x}_{ret} = \mathbf{A}^{-1} \mathbf{A}(\mathbf{x}_{true} - \mathbf{x}_a) \quad (2)$$

where  $\mathbf{x}_{ret}$ ,  $\mathbf{x}_a$ , and  $\mathbf{x}_{true}$  are vectors representing the altitude distributions of retrieved, a priori, and true species abundances. Rows of the matrix  $\mathbf{A}$  are the averaging kernels, each of which describes how differences between the true and a priori mixing ratio profiles

contribute to retrieved species abundance at a given altitude.

## 4. Results and Discussion

Figures 4 and 5 show HO<sub>2</sub> altitude profiles derived from the (figures 1 and 2, respectively) 260 and 254 GHz HO<sub>2</sub> spectra. Also shown in figures 4 and 5 are HO<sub>2</sub> profiles from the photochemical model. Formally, the retrieved profile should be compared with [Rodgers, 1990; Connor *et al.*, 1994]:

$$\hat{\mathbf{x}} = \mathbf{x}_a + \mathbf{A}(\mathbf{x}_{\text{model}} - \mathbf{x}_a) \quad (3)$$

rather than directly with the model. Comparison of equations 2 and 3 reveals that  $\hat{\mathbf{x}}$  is what the retrieval algorithm would find if the true [HO<sub>2</sub>] profile were given by  $\mathbf{x}_{\text{model}}$ . Because the a priori profile used for all our HO<sub>2</sub> retrievals is the standard photochemical model result using 1110(11) rate coefficients, the standard model [HO<sub>2</sub>] profile is identical to its corresponding  $\hat{\mathbf{x}}$  vector. The model result with 40% reduced  $k(\text{HO}_2 + \text{O} \rightarrow \text{OH} + \text{O}_2)$  differs from its corresponding  $\hat{\mathbf{x}}$  by -1.6% to -7% in figure 4, with a difference of -4% near 70 km, where the contribution functions (figure 3) peak. Differences between  $\mathbf{x}_{\text{model}}$  and corresponding  $\hat{\mathbf{x}}$  are similarly small for other retrievals; the  $\hat{\mathbf{x}}$  behavior relative to  $\mathbf{x}_{\text{model}}$  shown in figure 4 is representative.

Figures 1 and 2 show, in addition to the data, synthetic spectra corresponding to the retrieved and model [HO<sub>2</sub>] profiles. (A synthetic spectrum corresponding to a retrieved [HO<sub>2</sub>] profile is the best fit to the data.) It is clear that the standard photochemical model implies synthetic spectra well outside the noise of these measurements, and that the model result with 40% reduced  $k(\text{HO}_2 + \text{O} \rightarrow \text{OH} + \text{O}_2)$  is almost indistinguishable from the best fit to the data.

As discussed above, each photochemical 1110(11) calculation requires a water profile input, which we derive from a 203 GHz H<sub>2</sub><sup>18</sup>O observation. A representative H<sub>2</sub><sup>18</sup>O spectrum

is shown in figure 6. Figure 7 presents water profiles used as model inputs for the periods of HO<sub>2</sub> observations, and table 2 compares the Kitt Peak water vapor measurements with measurements made with the 22 GHz ground-based facility at Table Mountain, California [Nedoluha *et al.*, 1995; 1997] and with the Microwave Limb Sounder (MLS) on the Upper Atmospheric Research Satellite (UARS) [Lahoz, 1991; Lahoz *et al.*, 1996]

HO<sub>2</sub> observations were made at 255 GHz on April 11, 1992 and January 23, 1993, and at 260 GHz on April 3, November 30, and December 1 and 2, 1996. Measured mixing ratios for these observations for altitudes 50-80 km and local time 10am-2pm exceed those of the standard photochemical model by 47±12%, 40±10%, 26±7%, 23±5%, 30±7%, and 26±3%, respectively, where the stated uncertainties are one sigma s/n values. Other sources of error in the HO<sub>2</sub> measurements are calibration (5%) and the HO<sub>2</sub> pressure broadening coefficient (5%). The water vapor profile used as an input to the photochemical model contributes 8-10% uncertainty to the ratio of observed to model HO<sub>2</sub> abundances. From this, we conclude that observed HO<sub>2</sub> mixing ratios are 35±10% higher than model values in the lower mesosphere (50-80 km), in agreement with balloon measurements of a 30% HO<sub>2</sub> model deficit in the upper stratosphere (40-50 km). With the model reaction rate  $k(\text{HO}_2 + \text{O} \rightarrow \text{OH} + \text{O}_2)$  reduced by 40%, predicted HO<sub>2</sub> mixing ratios increase by 25-28% for the conditions on these six measurement dates, in agreement with measured values. Each of these observations was re-analyzed to obtain improved altitude resolution (with consequent increase in s/n uncertainty), as shown in figures 4 and 5. Table 3 summarizes this higher resolution analysis, with quoted mixing ratios at 60 and 70 km representing layers approximately 50-65 and 65-80 km, respectively.

#### 4.1 HO<sub>2</sub> Diurnal Behavior

A diurnal analysis was performed for observations made April 11, 1992 and January 23, 1993 at 255 GHz, as well as for observations made April 3 and November 30 - December 2, 1996 at 260 GHz. Long integrations, such as those represented by spectra in

---

figures 1 and 2, were broken into much shorter time intervals, obtaining high temporal resolution with lower  $s/n$ . Observations from the three days November 30 - December 2, 1996 were combined to give a single diurnal period, and spectra from that period corresponding to 30-60 minute intervals were individually fit. Longer time bins are required by the noisier observing conditions on other dates. Figures 8 and 9 show diurnally resolved  $\text{HO}_2$  measurements at 70 km, representing  $\text{HO}_2$  at altitudes 55-75 km, for January 23, 1993, and November 30 - December 2, 1996, respectively. Also shown are the corresponding photochemical model calculations for cases with standard chemistry and with 40% reduced  $k(\text{HO}_2 + \text{O} \rightarrow \text{OH} + \text{O}_2)$ . April 1992 and April 1996 diurnal results are similar.

$\text{HO}_2$  underprediction by the standard model is most clear and consistent near mid-day, when abundance is highest and spectral signal is strongest. The modified photochemical model clearly gives a better match to these mid-day observations than does the standard model. For three of the four diurnal analyses (excepting December 1996), model underprediction continues through the afternoon. The earliest morning (prior to  $\sim 9:30\text{am}$ )  $[\text{HO}_2]$  measurements are anomalously low on all four observation dates, and are better fit by the standard than modified model. Early evening  $[\text{HO}_2]$  measurements in January 1993 and December 1996 (the only two dates on which evening measurements were possible) are 100% higher than the standard model, and 4 to 6 sigma higher than even the modified model.

Measurements in early-mid morning through late afternoon are broadly consistent with the modified photochemical model and 40% reduction in  $k(\text{HO}_2 + \text{O} \rightarrow \text{OH} + \text{O}_2)$ . However, the early evening observations are clearly not explained by the model and merit further discussion.

Production of  $\text{HO}_x$  depends on photolysis of water and methane, as well as oxidation by  $\text{O}(^1\text{D})$ , itself a product of  $\text{O}_3$  photolysis.  $\text{HO}_x$  production thus stops at sunset and cannot be the cause of the sunset  $\text{HO}_2$  increase seen in figures 8 and 9. The remaining process to increase  $\text{HO}_2$  abundance is to shift the  $\text{HO}_x$  partitioning by conversion of

OH or H to HO<sub>2</sub>. A sudden jump in [HO<sub>2</sub>] at sunset is expected at 50--60 km due to the very rapid conversion of O to O<sub>3</sub> and sudden decline of O<sub>3</sub> photolysis as a source of O [eg Allen *et al.*, 1984, and the diurnal O<sub>3</sub> observations described below]. With the disappearance of atomic oxygen, the HO<sub>2</sub> + O → OH + O<sub>2</sub> conversion of HO<sub>2</sub> to OH ceases, while reaction of O<sub>3</sub> with OH to form HO<sub>2</sub> continues. However, this sunset partitioning of HO<sub>x</sub> to favor HO<sub>2</sub> at the expense of OH is less important at 70 km, where it is seen in the photochemical model (at higher time resolution than presented in figures 8 and 9) as a small effect. Because the pressure-broadened half-width of the HO<sub>2</sub> line below 60 km is ≥1 MHz, the narrow line observed at 6-7 pm (figure 10) rules out the possibility of a large repartitioning of OH to HO<sub>2</sub> at 50-60 km being misinterpreted as an increase in HO<sub>2</sub> at 70 km.

The following photochemical equilibrium expression for the [HO<sub>2</sub>] to [H] ratio may be derived from the HO<sub>x</sub> partitioning reactions R5, R6, R7, and R11:

$$\frac{[\text{HO}_2]}{[\text{H}]} = \frac{[\text{O}_2][\text{M}]}{k_6[\text{O}]} \quad (4)$$

Equation 4 is not expected to be rigorously true at sunset, because photochemical equilibrium conditions do not hold at that time. However, it does indicate that a large repartitioning of H to HO<sub>2</sub> will be driven by the rapid conversion of O to O<sub>3</sub> at sunset.

While the spectrum in figure 10 could be produced by very large HO<sub>2</sub> abundances above the 82 km maximum altitude of the photochemical model, the 1-2 hour decay of the observed evening HO<sub>2</sub> peak seen in the 1 December 1996 data indicates the signal must come from the 70-80 km altitude regime where HO<sub>x</sub> lifetime of one to several hours is consistent with the observed decay. The short lifetime of atomic oxygen (20 minutes at 70 km; 2 hours at 80 km) is consistent with rapid conversion of H to HO<sub>2</sub>. The strong altitude dependence of late afternoon mixing ratios of H and O (each increases one to two orders of magnitude from 70-80 km) and atomic oxygen lifetime within this altitude regime imply the evening jump in HO<sub>2</sub> abundance is a strong function of altitude. It is

possible the 2 km vertical resolution of the photochemical model is not adequate to fully capture this behavior. Model diurnal HO<sub>2</sub> mixing ratios shown in figure 11 illustrate the extreme altitude dependence of HO<sub>2</sub> behavior at dusk, particularly in the 76-78 km range.

The narrow 6-7pm emission line can only be produced by HO<sub>2</sub> above 70 km, where line width is dominated by (altitude independent) thermal broadening, and below 80 km, where chemical lifetimes are sufficiently short to allow the observed rapid change. We believe the observed very high post-sunset HO<sub>2</sub> abundances reflect a rapid conversion of 70-80 km H to HO<sub>2</sub> that is driven by partitioning of O to O<sub>3</sub>, and which is too strong a function of altitude to be represented in the photochemical model. Improved modeling of evening HO<sub>2</sub> behavior is a goal of future work.

#### 4.2 O<sub>3</sub> Diurnal Behavior

We also obtained high s/n measurements of the 2'19.7886 GHz O<sub>3</sub> line with 6-12 minute integrations. Figure 12 presents a typical spectrum. The observed O<sub>3</sub> emission line is significantly different from the synthetic spectrum corresponding to the standard theoretical ozone profile, as a consequence of the model ozone deficit. The synthetic O<sub>3</sub> spectrum corresponding to the modified model is nearly indistinguishable from the best fit spectrum, which parallels the behavior seen in the (figures 1 and 2) HO<sub>2</sub> behavior. Figure 13 shows O<sub>3</sub> altitude profiles corresponding to the spectra in figure 12. The retrieved O<sub>3</sub> altitude profile is consistent with the modified photochemical model and with the SME UV and IR monthly zonal means, but displays mixing ratios significantly higher than predicted with the standard photochemical model.

Diurnal O<sub>3</sub> behavior was measured January 23-25, 1993, by collecting eleven 249 GHz O<sub>3</sub> spectra and combining them to form a single diurnal period. Interleaving of the O<sub>3</sub> and HO<sub>2</sub> observations on January 23, 1993 leads to the gaps in HO<sub>2</sub> diurnal measurements shown in figure 8. Figures 14-16 present measured diurnal O<sub>3</sub> behavior at

three altitudes. Vertical error bars indicate uncertainty in derived mixing ratio, which are dominated by the effect of an 8% uncertainty in the collisional broadening coefficient. S/N uncertainty is very small, as reflected in the small vertical scatter of the measurements. The length of each observation was 6 or 12 minutes. The standard model O<sub>3</sub> deficit is evident throughout the day, and is consistent with the deficit seen in all comparable mesospheric O<sub>3</sub> data sets. Model underprediction of O<sub>3</sub> abundance increases with altitude (from 20% at 55 km to 40% at 65 km during daylight hours [Sandor et al., 1997]), and is substantially eliminated with the 40% reduced HO<sub>2</sub>+O rate coefficient. Simultaneous observations of diurnal HO<sub>2</sub> and O<sub>3</sub> behavior (figures 8 and 14-16) obtained in January 1993, demonstrate that the HO<sub>2</sub> and O<sub>3</sub> model deficits occur simultaneously.

The rapid drop in O<sub>3</sub> abundance at sunrise (figures 14-16) is due to photolysis of O<sub>3</sub> into O and O<sub>2</sub>; the rapid O<sub>3</sub> increase at sunset is driven by three body recombination of O with O<sub>2</sub>, and the sudden absence of photolytic O<sub>3</sub> loss. Because atomic oxygen abundances change much more quickly at twilight than do any of the HO<sub>x</sub> species abundances, the twilight HO<sub>x</sub> chemistry is largely driven by these changes in atomic oxygen, as discussed in the preceding section in the context of observed very large post-sunset HO<sub>2</sub> abundances.

## 5. Summary

Microwave spectra of HO<sub>2</sub>, O<sub>3</sub>, and H<sub>2</sub><sup>18</sup>O are inverted to retrieve mixing ratios of HO<sub>2</sub>, O<sub>3</sub>, and H<sub>2</sub>O in the upper stratosphere and mesosphere (45-80 km). The focus of this study is on mesospheric HO<sub>2</sub>, which is uniquely determined with methods described in this paper. Emission line shapes have been fit to obtain altitude resolution of 10-15 km within the 45-80 km range. HO<sub>2</sub> and O<sub>3</sub> observations are binned into integrations of 30 minutes - 2 hours and 6 - 12 minutes, respectively, to characterize the diurnal variability of each species. H<sub>2</sub>O abundance derived from H<sub>2</sub><sup>18</sup>O observations has been used as an input to a diurnal photochemical model, with which theoretical HO<sub>2</sub> and O<sub>3</sub> abundances

are calculated for comparison with the observations.

The present work is an updated study, expanding on the initial data and analysis reported by *Clancy et al.* [1994a]. Improvements include use of data from additional observations made since the *Clancy et al.* [1994a] analysis. Hardware improvements have enabled observations of an HO<sub>2</sub> line at 260 GHz that is 58% stronger than the 254 GHz line used previously. Laboratory spectroscopic studies have provided values for the hyperfine splitting of HO<sub>2</sub> lines [*Chance et al.*, 1995; 1997; *K. Chance, personal communication 1997*] as well as increased confidence in the estimated 102 pressure broadening coefficient [*Nelson and Zahniser*, 1994]. The zero dimensional photochemical model [*Rusch and Eckman*, 1985] employed by *Clancy et al.* [1994] has been substantially improved [*Siskind et al.*, 1995], with the model's upper altitude limit extended to 82 km. The Kitt Peak facility's absolute calibration, designed for astronomical observations, has also been revised for atmospheric observations [*Sandor and Clancy*, 1997].

O<sub>3</sub> abundances observed at Kitt Peak are consistent with other observational data sets, such as the SME IR [*Thomas et al.*, 1984] and UV [*Rusch et al.*, 1983] monthly zonal means, but are 20%-40% higher than the model predicted values (figures 14-16), where the model vs data disagreement increases with altitude. This model underprediction is consistent with the long-standing ozone deficit problem [*Solomon et al.*, 1983], as modified by changes to HO<sub>x</sub> loss rates [*e.g. Clancy et al.*, 1987]. O<sub>3</sub> diurnal observations show model underprediction is consistent throughout the day. Mid-day 50-80 km HO<sub>2</sub> observed abundances, which provide the strongest signal and therefore best S/N, are 23% to 47% higher than model prediction. HO<sub>2</sub> observations are consistent with the standard model for roughly 7 to 9 am, and are 100% higher than model prediction for 6-7pm, just after sunset. Model HO<sub>2</sub> values for 9am to 6pm, as well as O<sub>3</sub> values for all times of day, are brought into agreement with the model for a 40% (two sigma relative to JPL94 recommendations) decrease in the value of the reaction rate coefficient,  $k(\text{HO}_2 + \text{O} \rightarrow \text{OH} + \text{O}_2)$ . Other consequences of this rate coefficient change

include (1) decreased model OH, resulting in improved agreement with MAHRSI measurements [Summers *et al.*, 1997], (2) increased model CO, improving agreement with ground-based microwave observations [Solomon *et al.*, 1985], (3) increased upper mesospheric model temperatures, again improving agreement with data [Siskind *et al.*, 1996], and (4) reduction of the model ozone deficit at 40-50 km altitude [Khosravi *et al.*, 1997]. This rate change has negligible effect on lower stratospheric chemistry [Chin *et al.*, 1997; Summers *et al.*, 1997].

The factor of two model HO<sub>2</sub> underprediction at dusk is not resolved by the rate coefficient change. We believe this problem may indicate that twilight chemistry between 70 and 80 km is too strong a function of altitude to be adequately represented with the model's 2 km altitude resolution.

**Acknowledgments.** We gratefully acknowledge the assistance of NRAO staff at Kitt Peak. (The National Radio Astronomy Observatory is operated by Associated Universities, Inc., under cooperative agreement with the National Science Foundation.) In particular, we thank Jeff Mangum and Phil Jewell for their constant technical support of our observations and NRAO telescope operators Duane Clark, Lisa Engle, Victor Glasho, Paul Hart, Harry Stahl, and Ed Treiber for their invaluable operational support. We also thank Dave Rusch and Susan Solomon for scientific discussions. Investigators Sandor and Clancy were supported by the NSF grant ATM-9501288 toward completion of this research. The research described in this paper was partially performed while B. J. Sandor held a National Research Council-NASA Resident Research Associateship award at the Jet Propulsion Laboratory, California Institute of Technology, under contract with the National Aeronautics and Space Administration.

## References

- Allen, M., J.I. Lunine, and Y.L. Yung, The vertical distribution of ozone in the mesosphere and lower thermosphere, *J. Geophys. Res.*, *89*, 4841-4872, 1984.
- Brasseur, G., and S. Solomon, *Aeronomy of the Middle Atmosphere*, 452 pp., D. Reidel, 1986.
- Chance, K., P. de Natale, M. Bellini, M. Inguscio, G. di Leonardo, and L. Fusina, Pressure Broadening of the 2.4978- THz Rot ational Lines of HO<sub>2</sub> by N<sub>2</sub> and O<sub>2</sub>, *J. Molec. Spectr.*, *163*, 67-70, 1994.
- Chance, K. V., K. Park, K.M. Evenson, L.R. Zink, and F. Stroh, Far-infrared spectrum of HO<sub>2</sub>, *J. Molec. Spectr.*, *172*, 407-420, 1995.
- Chance, K. V., K. Park, K.M. Evenson, L.R. Zink, F. Stroh, E.H. Fink, and D. A. Ramasay, Note: Improved molecular constants for the ground state of HO<sub>2</sub>, *J. Molec. Spectr.*, *183*, 418, 1997.
- Clancy, R.T., D.W. Rusch, R.J. Thomas, M. Allen, and R. S. Eckman, Model ozone photochemistry on the basis of solar mesospheric explorer mesospheric observations, *J. Geophys. Res.*, *92*, 30673080, 1987.
- Clancy, R.T., D.W. Rusch, and D.O. Muhleman, A microwave measurement of high levels of thermospheric nitric oxide, *Geophys. Res. Lett.*, *19*, 26126-31, 1992.
- Clancy, R.T., and D.O. Muhleman, Ground-based microwave spectroscopy of the earth's stratosphere and mesosphere, in *Atmospheric Remote Sensing by Microwave Radiometry*, edited by M. A. Janssen, pp. 335-382, John Wiley, New York, 1993.
- Clancy, R.T., B.J. Sandor, D.W. Rusch, and D.O. Muhleman, Microwave observations and modeling of O<sub>3</sub>, H<sub>2</sub>O, and HO<sub>2</sub> in the mesosphere, *J. Geophys. Res.*, *99*, 5465-5473, 1994a.
- Clancy, R.T., D.W. Rusch, and M.T. Callan, Temperature minima in the average thermal structure of the middle atmosphere (70-80 km) from analysis of 40- to 92- km SME global temperature profiles, *J. Geophys. Res.*, *99*, 19,001-19,020, 1994b.
- Chin, M., R. Stolarski, and D. Considine, A Monte Carlo study of radical diurnal variations during SPADÉ observation (abstract), *EOS*, *78* (17), Spring Meet. Suppl., S80, 1997.
- Connor, B.J., D.E. Siskind, J.J. Tsou, A. Parrish, and E.E. Remslberg, Ground-based observa-

- tions of ozone in the upper stratosphere and mesosphere, *J. Geophys. Res.*, *99*, 16,757- 16,770, 1994.
- Conway, R.R., M.H. Stevens, J.G. Cardon, S.E. Zasadil, C.M. Brown, J.S. Morrill, and G.H. Mount, Satellite measurements of hydroxyl in the mesosphere, *Geophys. Res. Lett.*, *23*, 2093-2096, 1996.
- DeMore, W. B., S. P. Sander, D. M. Golden, R. F. Hampson, M. J. Kurylo, C. J. Howard, A. R. Ravishankara, C. E. Kolb, and M. J. Molina, *Chemical kinetics and photochemical data for use in stratospheric modeling*, *JPL Publ. 94-26*, Jet Propul. Lab., Pasadena, Calif., 1994.
- de Zafra, R.L., A. Parrish, P.M. Solomon, and J.W. Barrett, A measurement of stratospheric HO<sub>2</sub> by ground-based millimeter-wave spectroscopy, *J. Geophys. Res.*, *89*, 1321- 1326, 1984.
- Fluszkiewicz, J., and M. Allen, A global analysis of the ozone deficit in the upper stratosphere and lower mesosphere, *J. Geophys. Res.*, *98*, 1069- 1082, 1993.
- Fleming, E.L., S. Chandra, J.J. Barnett, and M. Corney, Pressure, zonal wind, and geopotential height as functions of latitude, in *COSPAR International Reference Atmosphere: 1986*, part II, *Middle Atmosphere Models*, edited by D. Rees, J.J. Barnett, and K. Labitzke, pp. 11- 59, Pergamon, New York, 1990.
- Kaye, J. A., Mechanisms and observations for isotope fractionation of molecular species in planetary atmospheres, *Rev. Geophys.*, *25*, 1609-1658, 1987.
- Khosravi, G.J., Brasseur, A.K. Smith, D.W. Rusch, J.W. Waters, and J.M. Russell, Significant reduction in the ozone deficit: A 3-D model study using UARS data (abstract), *EOS*, *78* (17), Spring Meet. Suppl., S97, 1997.
- Lahoz, W. A., The 183 GHz water and ozone channels on the Upper Atmospheric Research Satellite microwave limb sounder, *Int. J. Rem. Sensing*, *12*, 33-53, 1991.
- Lahoz, W. A., et al., Validation of UARS MLS 183 GHz H<sub>2</sub>O measurements, *J. Geophys. Res.*, *101*, 10,129- 10,140, 1996.
- Nedoluha, G.E., R. M. Bevilacqua, R. M. Gomez, D.L. Thacker, W.B. Waltman, and J. A. Pauls, Ground-based measurements of water vapor in the middle atmosphere, *J. Geophys. Res.*, *100*, 2927- 2939, 1995.
- Nedoluha, G.E., R.M. Bevilacqua, R. M. Gomez, D.E. Siskind, and B. Hicks, Increases in mid-

- de atmospheric water vapor as observed by HALOE and the ground-based Water Vapor Millimeter-wave Spectrometer from 1991-1997, *J. Geophys. Res.*, , submitted, 1997.
- Nelson, D.D., Jr., and M.S. Zahniser, Air-broadened linewidth measurements in the  $\nu_2$  vibrational band of the hydroperoxyl radical, *J. Molec. Spectr.*, *166*, 273-279, 1994.
- Park, J.H. and B. Carli, Spectroscopic measurements of HO<sub>2</sub>, H<sub>2</sub>O<sub>2</sub>, and OH in the stratosphere, *J. Geophys. Res.*, *96*, 22,535-22,541, 1991.
- Pickett, H. M., and D.B. Peterson, Comparison of measured stratospheric OH with prediction, *J. Geophys. Res.*, *101*, 16,789-16,796, 1996.
- Pickett, H. M., R.L. Poynter, E. A. Cohen, M.J. Delitsky, J.C. Pearson, and H. S.P. Muller, *Submillimeter, millimeter, and microwave spectral line catalog*, JPL Publ. 80-23, Jet Propul. Lab., Pasadena, Calif., 1996.
- Poynter, R.L., and H.M. Pickett, Submillimeter, millimeter, and microwave spectral line catalog, *Appl. Opt.*, *24*, 2235-2240, 1985.
- Rodgers, C.D., Characterization and error analysis of profiles retrieved from remote sounding measurements, *J. Geophys. Res.*, *95*, 5587-5595, 1990.
- Rothman, L.S. et al., The HITRAN Molecular Database: Editions of 1991 and 1992, *J. Quant. Spectrosc. Radiat. Transf.*, *48*, 469-507, 1992.
- Rusch, D. W., and D. S. Eckman, Implications of the comparison of ozone abundances measured by the Solar Mesospheric Explorer to model calculations, *J. Geophys. Res.*, *90*, 12,991-12,998, 1985.
- Rusch, D. W., G.H. Mount, C.A. Barth, G.J. Rottman, R.J. Thomas, G.E. Thomas, R.W. Sanders, G.M. Lawrence, and D. S. Eckman, Ozone densities in the lower mesosphere measured by a limb scanning ultraviolet spectrometer, *Geophys. Res. Lett.*, *10*, 241, 1983.
- Sandor, B. J., R.T. Clancy, D. W. Rusch, C.F. Randall, R.S. Eckman, D.S. Siskind, and D.O. Muhleman, Microwave observations and modeling of OZ(113F<sub>2</sub>) and O<sub>3</sub> diurnal variation in the mesosphere, *J. Geophys. Res.*, *102*, 9013-9028, 1997.
- Sandor, D.O., and D.P. Clancy, Mesospheric observations and modeling of the Zeeman split 233.9 GHz <sup>18</sup>O<sup>16</sup>O line, *Geophys. Res. Lett.*, *24*, 1627-1631, 1997.
- Siskind, D.F., B.J. Comor, D.S. Eckman, E.E. Remsberg, J.L. Tsou, and A. Parrish, An inter-

- comparison of model ozone deficits in the upper stratosphere and mesosphere from two data sets, *J. Geophys. Res.*, *100*, 11,191–11,201, 1995.
- Siskind, D. E., M.E. Summers, J.T. Bacmeister, and R.R. Conway, On the contribution of exothermic chemistry to the thermal budget at mesopause altitudes (abstract), *EOS*, *77* (17), Spring Meet. Suppl., S186, 1996.
- Solomon, S., D.W. Rusch, R.J. Thomas, and H.S. Eckman, Comparison of mesospheric ozone abundances measured by the solar mesospheric explorer and 1110(1) calculations, *Geophys. Res. Lett.*, *10*, 249–252, 1983.
- Solomon, S., R.R. Garcia, J.J. Olivero, R.M. Bevilacqua, P.R. Schwartz, M.P. Clancy, and D.O. Muhleman, Photochemistry and transport of carbon monoxide in the middle atmosphere, *J. Atmos. Sci.*, *42*, 1072–1083, 1985.
- Stachnik, R. A., J.C. Hardy, J. A. Tarsala, J.W. Waters, and N. H. Erickson, Submillimeterwave heterodyne measurements of stratospheric ClO, HCl, O<sub>3</sub>, and HO<sub>2</sub>: First results, *Geophys. Res. Lett.*, *19*, 1931–1934, 1992.
- Stimpfle, R.M., P.O. Wennberg, L.B. Lapsen, and J.G. Anderson, Simultaneous, in situ measurements of OH and HO<sub>2</sub> in the stratosphere, *Geophys. Res. Lett.*, *17*, 1905–1908, 1990.
- Summers, M.E., R.R. Conway, D.E. Siskind, R.M. Bevilacqua, D.F. Strobel, and S. Zasadil, Mesospheric HO<sub>x</sub> photochemistry: Constraints from recent satellite measurements of OH and H<sub>2</sub>O, *Geophys. Res. Lett.*, *23*, 2097–2100, 1996.
- Summers, M.E., R.R. Conway, D.E. Siskind, M.H. Stevens, D. Offermann, M. Riese, P. Preuse, D.F. Strobel, and J.M. Russell III, Implications of satellite hydroxyl observations for middle atmospheric water vapor and ozone chemistry, *Science*, *in press*, , 1997.
- Thomas, R.J., C.A. Barth, D.W. Rusch, and R.W. Sanders, Solar Mesosphere Explorer near-infrared spectrometer: Measurements of 1.27 $\mu$ m radiances and the inference of mesospheric ozone, *J. Geophys. Res.*, *89*, 9569–9580, 1984.
- Traub, W.A., D.G. Johnson, and K.V. Chance, Stratospheric hydroperoxyl measurements, *Science*, *247*, 446–449, 1990.

**Figure 1.** 260 GHz  $\text{HO}_2$  spectrum observed 10:00-14:00 local time, averaged over three days November 30 - December 2, 1996. Also shown are synthetic spectra corresponding to the best-fit (solid), standard photochemical model  $[\text{HO}_2]$  altitude profile (dotted), and photochemical model with 40% reduced  $k(\text{HO}_2 + \text{O})$  (dashed). The standard model synthetic spectrum demonstrates model underprediction of  $[\text{HO}_2]$ . The reduced  $k(\text{HO}_2 + \text{O})$  synthetic spectrum is almost identical to the best fit.

**Figure 2.** Same as figure 1, but for a 255 GHz  $\text{HO}_2$  spectrum, observed 07:15-17:30, January 23, 1993.

**Figure 3.**  $\text{HO}_2$  260 GHz contribution functions. These indicate the source altitude and relative weightings of contributions to observed spectra. For example, the difference between signal at 0.125 and 1.125 MHz from line center (dotted curve) is most sensitive to emission from  $\sim 62$ -74 km. These contribution functions are the weighting functions in Clancy *et al.*, [1994a], multiplied by the  $\text{HO}_2$  mixing ratio.

**Figure 4.**  $\text{HO}_2$  mixing ratios corresponding to the 260 GHz spectra shown in figure 1. Dotted profile is the standard photochemical model result and is the a priori profile used for the retrieval. Dashed line is the photochemical model result with rate coefficient for  $\text{HO}_2 + \text{O}$  reduced 40%. The dot-dashed line shows the profile that would be retrieved (the  $\hat{x}$  values defined by equation 3) if the true profile were the dashed profile.

**Figure 5.**  $\text{HO}_2$  mixing ratios corresponding to the 254 GHz spectra shown in figure 2. Dotted profile is the standard photochemical model result and is the a priori profile used for the retrieval. Dashed line is the photochemical model result with rate coefficient for  $\text{HO}_2 + \text{O}$  reduced 40%.

**Figure 6.** The 203 GHz spectrum of  $\text{H}_2^{18}\text{O}$ , observed April 10, 1992. The 250 KHz resolution data are represented by the histogram. The dashed curve is the best fit to the data.

Figure 7.  $\text{H}_2\text{O}$  altitude profiles retrieved from observations on the indicated dates. Error bars on each profile represent 1-sigma S/N uncertainties for altitude bins 48-58 and 58-70 km. No  $\text{H}_2^{18}\text{O}$  observation was made in April 1996; the solid curve (presented without error bars) indicates climatological values for that date used as input to the photochemical model. Dotted curve, April 10, 1992. Dashed curve, January 23, 1993. Solid curve, April 3, 1996. Dot-dashed curve, December 2, 1996.

**Figure 8.** 55-75 km diurnal  $\text{HO}_2$  behavior on January 23, 1993. Solid horizontal lines indicate retrieved mixing ratio at 70 km, and have length corresponding to the duration of each observation. Solid vertical lines indicate the 1-sigma s/n error. Dotted horizontal lines indicate the standard photochemical model values. Dashed horizontal lines indicate model values with  $k(\text{HO}_2 + \text{O}) \rightarrow \text{OH} + \text{O}_2$  reduced 40%.

Figure 9. Same as figure 8, but for 260 GHz observations on November 30- December 2, 1996. Data from the three days have been collected into a single diurnal period, improving s/n to allow better time resolution (30-90" minutes).

**Figure 10.** 260 GHz  $\text{HO}_2$  spectrum, observed 6-7pm, November 30 - December 2, 1996.

**Figure 11.** Model  $\text{HO}_2$  diurnal mixing ratios for December 1, 1996. Altitude dependence of  $\text{HO}_2$  time behavior is very strong, particularly just after sunset.

**Figure 12.** The 249 GHz spectrum of  $O_3$ , observed at 1300 LT, April 10, 1992. The 250 KHz resolution data are represented by the histogram. The dashed curve is the best fit to the data, and the dotted curve is the synthetic emission line corresponding to the standard photochemical model  $O_3$  altitude profile. Plus's indicate the synthetic spectrum corresponding to the photochemical model  $O_3$  profile for  $k(HO_2 + O \rightarrow OH + O)$  reduced 40%; this spectrum is almost indistinguishable from the best fit.

**Figure 13.** Representative  $O_3$  altitude profile. The solid curve was derived from the 249 GHz data shown in Figure 12. Error bars indicate pressure broadening, calibration, and 1-sigma S/N uncertainties for altitude bins 48-58 and 58-72 km. The dotted line is the standard photochemical model result, corresponding to the dotted line spectrum in Figure 10. The dashed line is the photochemical model result with the indicated rate change, corresponding to the plus's in figure 12. Also shown are the 4-year monthly mean values derived from SME IR [Thomas *et al.*, 1984] and UV [Rusch *et al.*, 1983] observations.

**Figure 14.** Diurnal behavior of  $O_3$  on January 23-25, 1993. Crosses indicate the retrieved mixing ratios at 52 km for a two-layer (48-58 and 58-72 km) fit to the observations, with horizontal bar indicating the length of the observation (6-12 min) and vertical bar indicating the uncertainty of the derived value. Errors bars are dominated by pressure-broadening uncertainty. The solid curve represents the standard photochemical model  $O_3$  behavior. The dashed curve indicates the photochemical model result for the case in which  $k(HO_2 + O \rightarrow OH + O_2)$  is reduced 40% below the JPL94 value. The 4-year zonal monthly mean values determined from SME UV (dot-dashed line) and IR (1.27  $\mu m$ , dotted line) observations are shown at the middle to late afternoon time period during which those observations were made.

**Figure 15.** Same as Figure 14 for 60 km.

**Figure 16.** Same as Figure 14 for 68 km.

**Table 1.** HO<sub>x</sub> and O<sub>x</sub> Reactions

Reaction	Rate
J1 O <sub>2</sub> + hν → O + O	λ < 242nm
J2a O <sub>3</sub> + hν → O <sub>2</sub> + O	λ < 310nm
J2b O <sub>3</sub> + hν → O <sub>2</sub> + C	λ < 1140nm
J3 H <sub>2</sub> O + hν → H + OH	λ < 242nm
J4 H <sub>2</sub> O <sub>2</sub> + hν → C + OH	λ < 870nm
R1 H <sub>2</sub> O + O( <sup>1</sup> D) → 2OH	2.2 × 10 <sup>-10</sup>
R2 H <sub>2</sub> + O( <sup>1</sup> D) → H + OH	1.0 × 10 <sup>-10</sup>
R3 H + HO <sub>2</sub> → H <sub>2</sub> + O <sub>2</sub>	8.1 × 10 <sup>-12</sup>
R4 OH + HO <sub>2</sub> → H <sub>2</sub> O + O <sub>2</sub>	4.8 × 10 <sup>-11</sup> e <sup>250/T</sup>
R5 C + O → H + O <sub>2</sub>	2.2 × 10 <sup>-11</sup> e <sup>120/T</sup>
R6 HO <sub>2</sub> + O → C + O <sub>2</sub>	3.0 × 10 <sup>-11</sup> e <sup>200/T</sup>
R7 H + O <sub>2</sub> + M → HO <sub>2</sub> + M	5.7 × 10 <sup>-32</sup> (T/300) <sup>-1.6</sup>
R8 O + O <sub>3</sub> → 2O <sub>2</sub>	8.0 × 10 <sup>-12</sup> e <sup>2060/T</sup>
R10 O + O <sub>2</sub> + M → O <sub>3</sub> + M	6.0 × 10 <sup>-34</sup> (T/300) <sup>-2.3</sup>
R11 H + O <sub>3</sub> → OH + O <sub>2</sub>	1.4 × 10 <sup>-10</sup> e <sup>470/T</sup>
R12 O + O <sub>3</sub> → HO <sub>2</sub> + O <sub>2</sub>	1.6 × 10 <sup>-12</sup> e <sup>910/T</sup>
R13 C + e → H <sub>2</sub> O + C	4.2 × 10 <sup>-12</sup> e <sup>240/T</sup>
R14 C <sub>2</sub> + HO <sub>2</sub> → H <sub>2</sub> O <sub>2</sub> + O <sub>2</sub>	2.3 × 10 <sup>-13</sup> e <sup>600/T</sup>
R15 HO <sub>2</sub> + O <sub>3</sub> → 2O <sub>2</sub> + O <sub>1</sub>	1.1 × 10 <sup>-14</sup> e <sup>500/T</sup>
R16 H <sub>2</sub> O <sub>2</sub> + OH → H <sub>2</sub> O + HO <sub>2</sub>	2.9 × 10 <sup>-12</sup> e <sup>160/T</sup>

HO<sub>x</sub> and O<sub>x</sub> reactions used in photochemical model.

Rates are JPL94, in cgs units. Model runs also include NO<sub>x</sub> and ClO<sub>x</sub> chemistry not listed here.

**Table 3.** HO<sub>2</sub> 10-15 km vertical resolution data-model comparison.

Date	Time, LST	$\mu$ wave HO <sub>2</sub> (ppbv)		HO <sub>2</sub> (observed)/HO <sub>2</sub> (model)			
		@70km	@60km	JPL94 rates		0.6×k(HO <sub>2</sub> +O)	
				@70km	@60km	@70km	@60km
11 Apr92	<b>0800-1600</b>	3.59±0.85	0.67±0.36	1.55±0.42	0.92±0.50	1.17±0.31	0.68±0.38
23 Jan93	<b>0715-1730</b>	2.48±0.54	0.58±0.18	<b>1.49±0.39</b>	1.08±0.36	1.13±0.31	0.79±0.27
3 Apr96	<b>0730-1800</b>	2.98±0.46	0.75±0.18	1.38±0.29	1.09±0.29	1.04±0.22	<b>0.80±0.21</b>
30 Nov96	<b>1000-1400</b>	2.37±0.54	0.95±0.14	1.09±0.29	1.35±0.26	0.82±0.22	1.00±0.19
1 Dec96	<b>10(K)-1400</b>	3.01±0.83	0.89±0.23	<b>1.38±0.43</b>	<b>1.28±0.36</b>	1.04±0.32	0.94±0.27
2 Dec96	<b>1000-1400</b>	3.03±0.31	0.78±0.15	<b>1.39±0.21</b>	1.12±0.18	1.05±0.18	<b>0.82±0.13</b>
30 Nov -2 Dec96	<b>1000-1400</b>	2.86±0.28	0.85±0.09	1.31±0.22	1.21±0.19	0.99±0.17	<b>0.83±0.14</b>

Summary of HO<sub>2</sub> measurements. Long observations allow retrievals with best altitude resolution. Measurement uncertainty (σ) in columns 3 and 4 are the one-sigma/σ errors. Uncertainties in the data-to-photochemical model ratios (columns 5-8) include these σ errors, as well as uncertainties due to pressure broadening (0-8%), calibration (5%), temperature profile (3%), and model water profile (10%). 1992-1993 observations were made at 255 GHz, and 1996 observations at 260 GHz.

Fig 1. \* 260GHz HO<sub>2</sub> 10am - 20m, 30Nov - 2Dec96

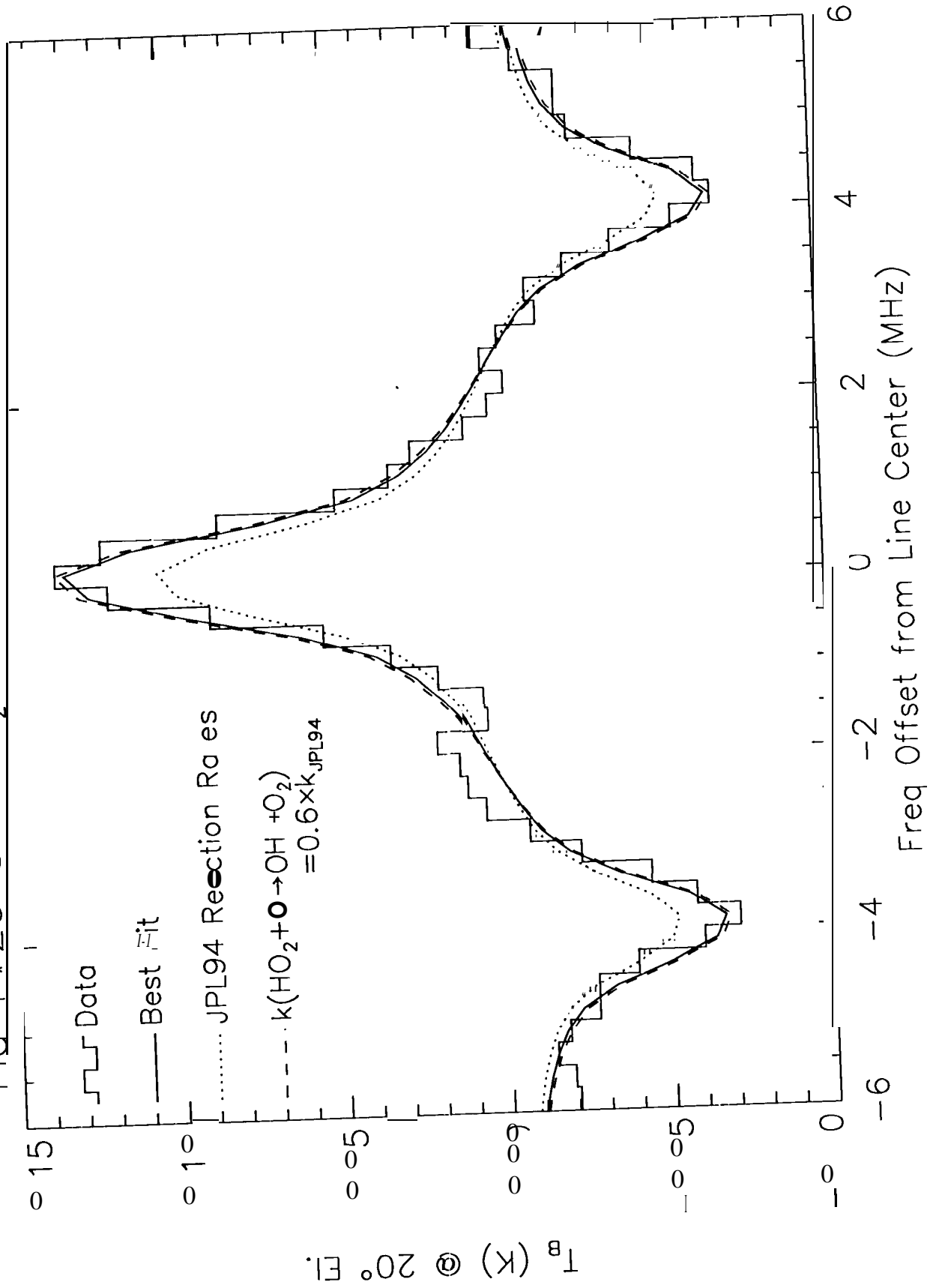


Fig 2: 255GHz, 07:15am-5:30pm, 23 Jan93

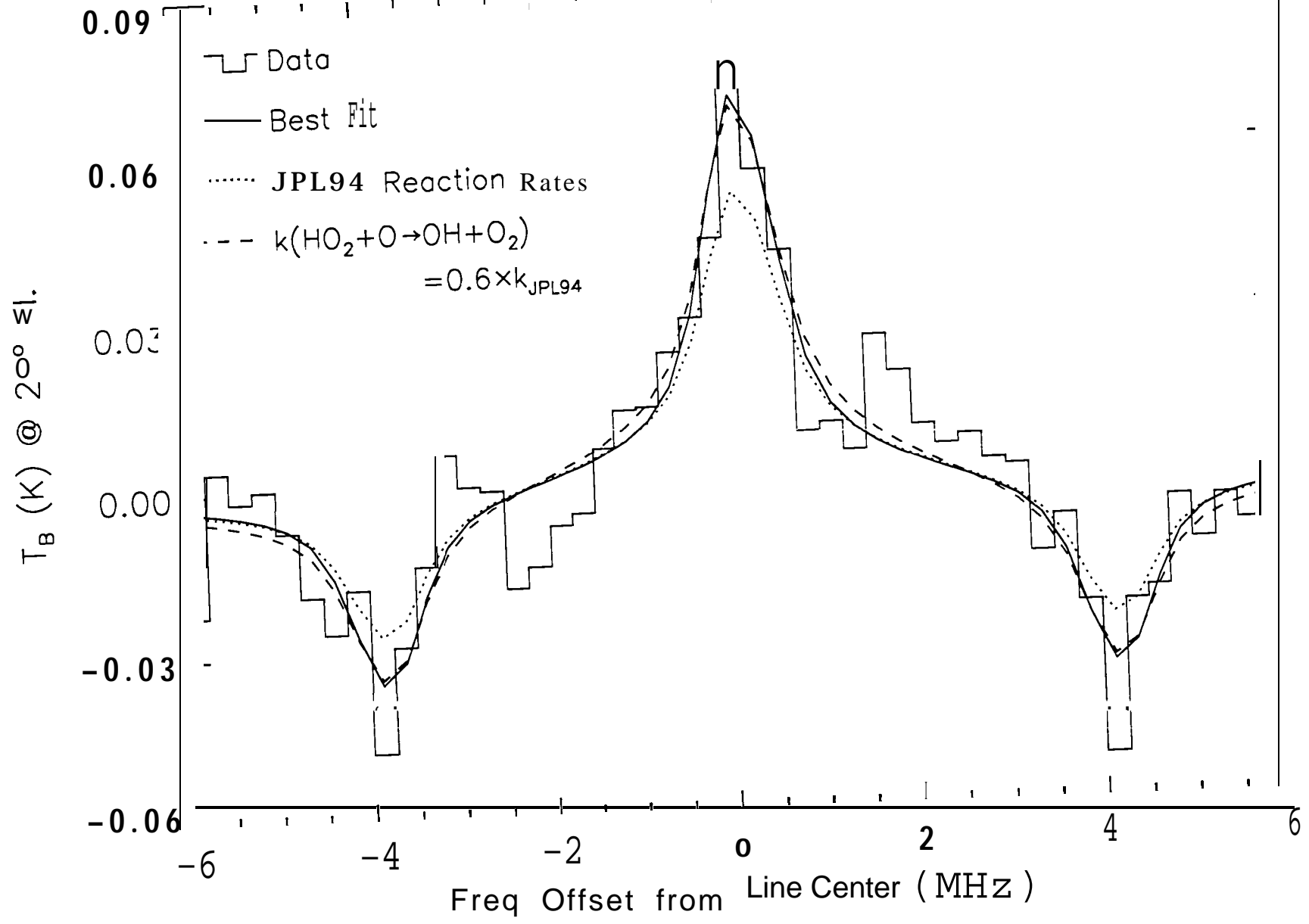


Fig 3: HO<sub>2</sub> 260 GHz **Contribution Functions**

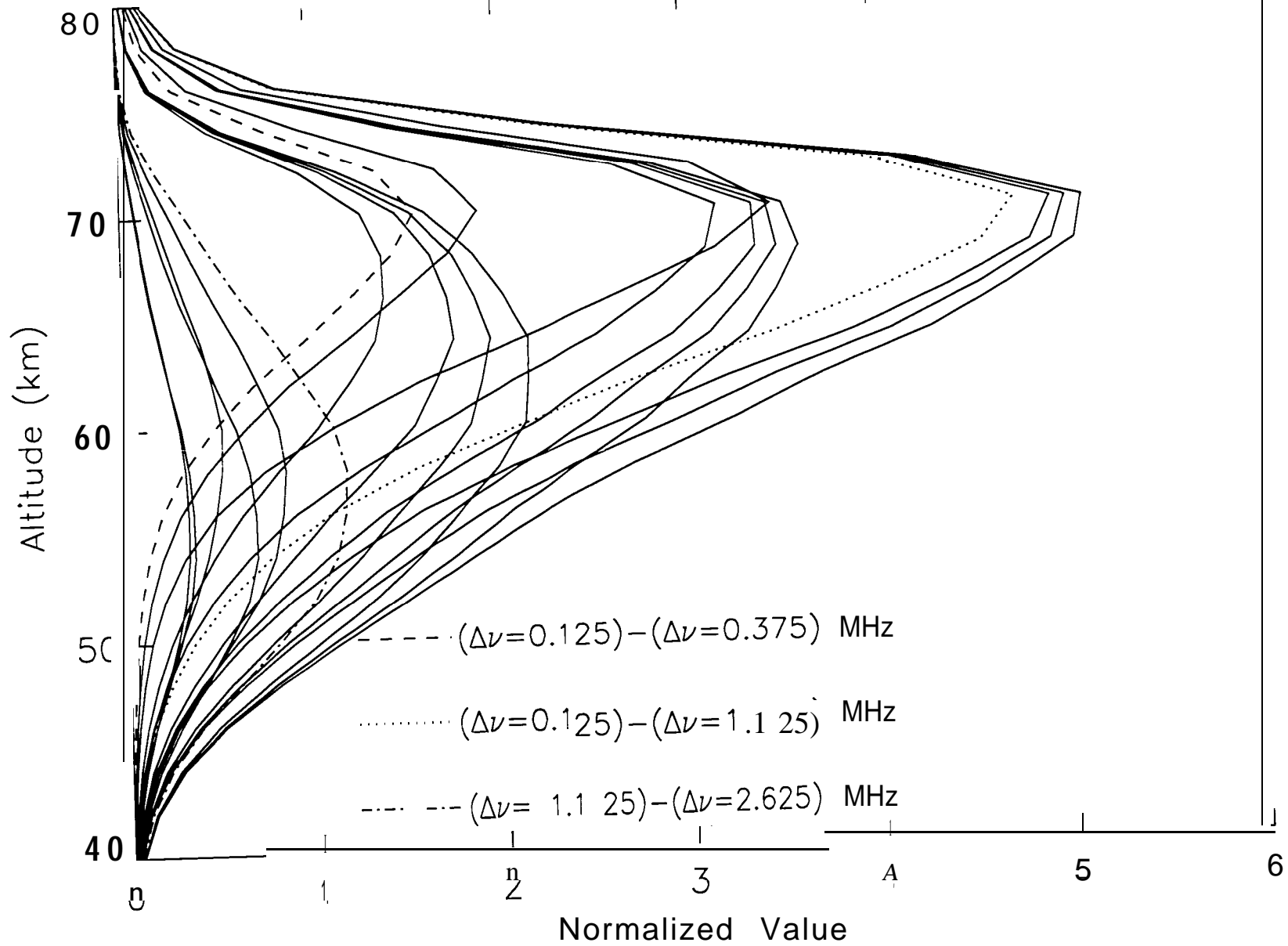


Fig 4. 30Nov-2Dec96 HO<sub>2</sub>, 10am-2pm

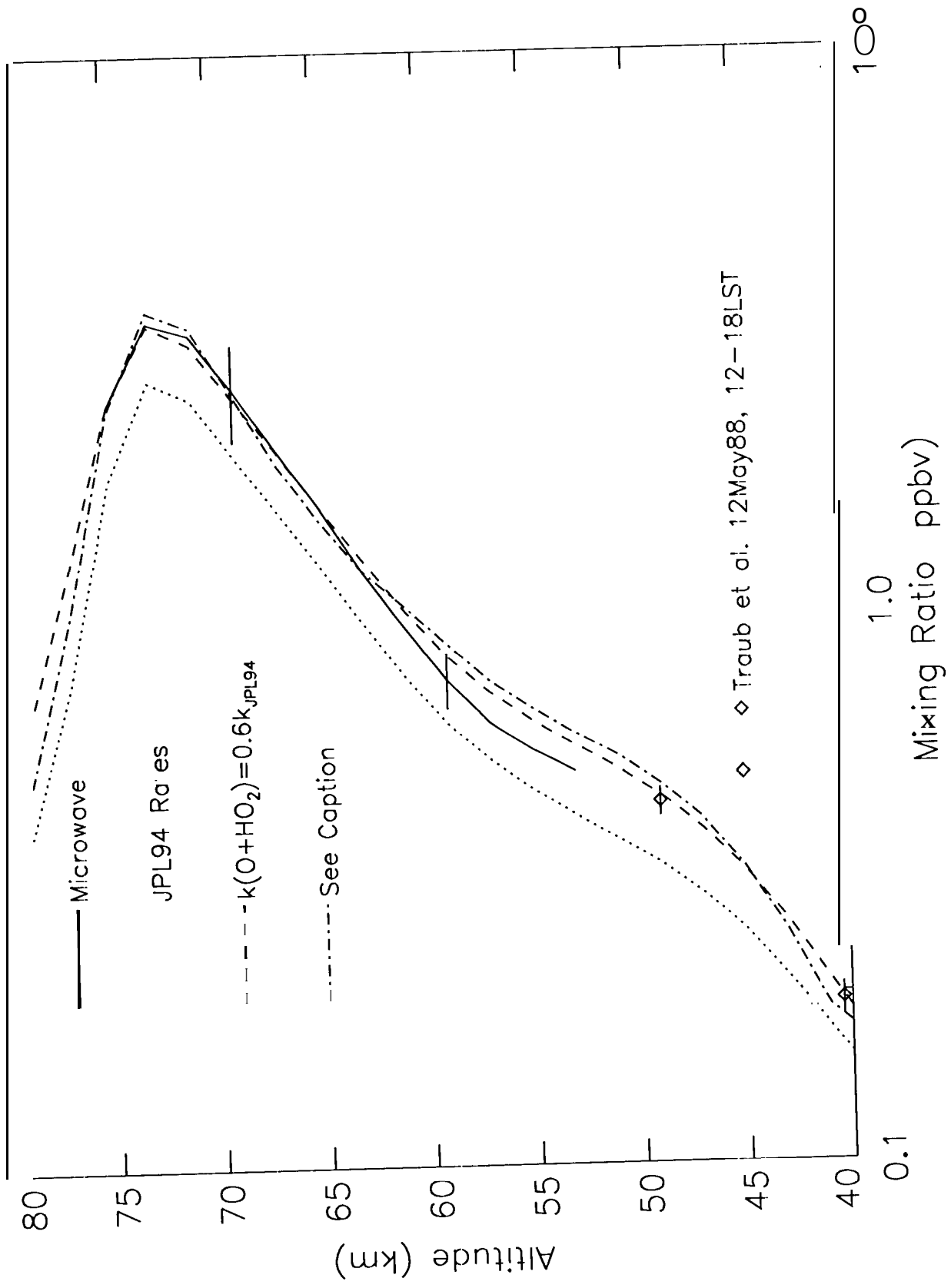


Fig 5: 23 Jan 93 HO<sub>2</sub>, 7:15am - 5:30pm, ,

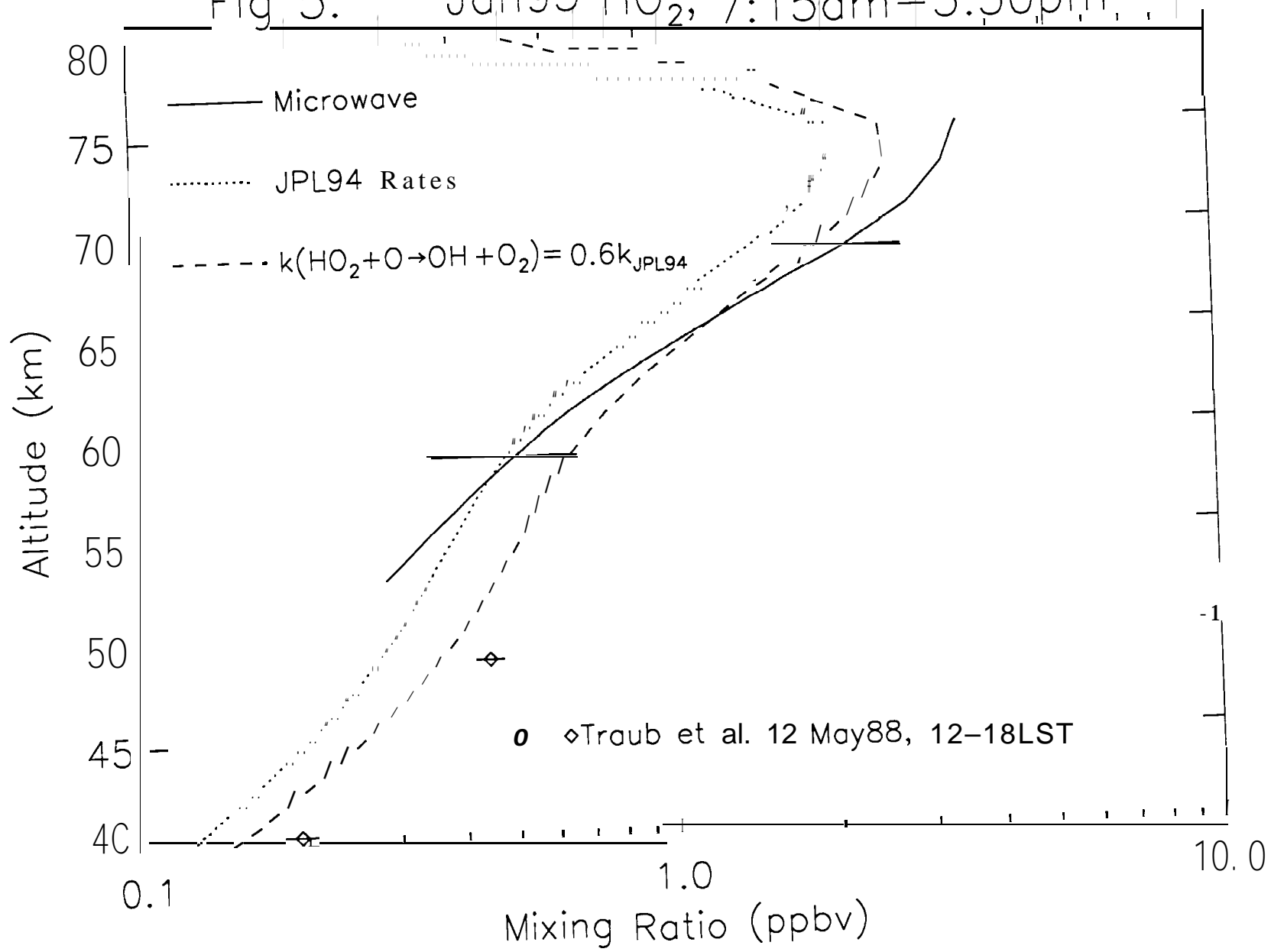


Fig 6. 203GHz H<sub>2</sub><sup>18</sup>O, 10Apr92

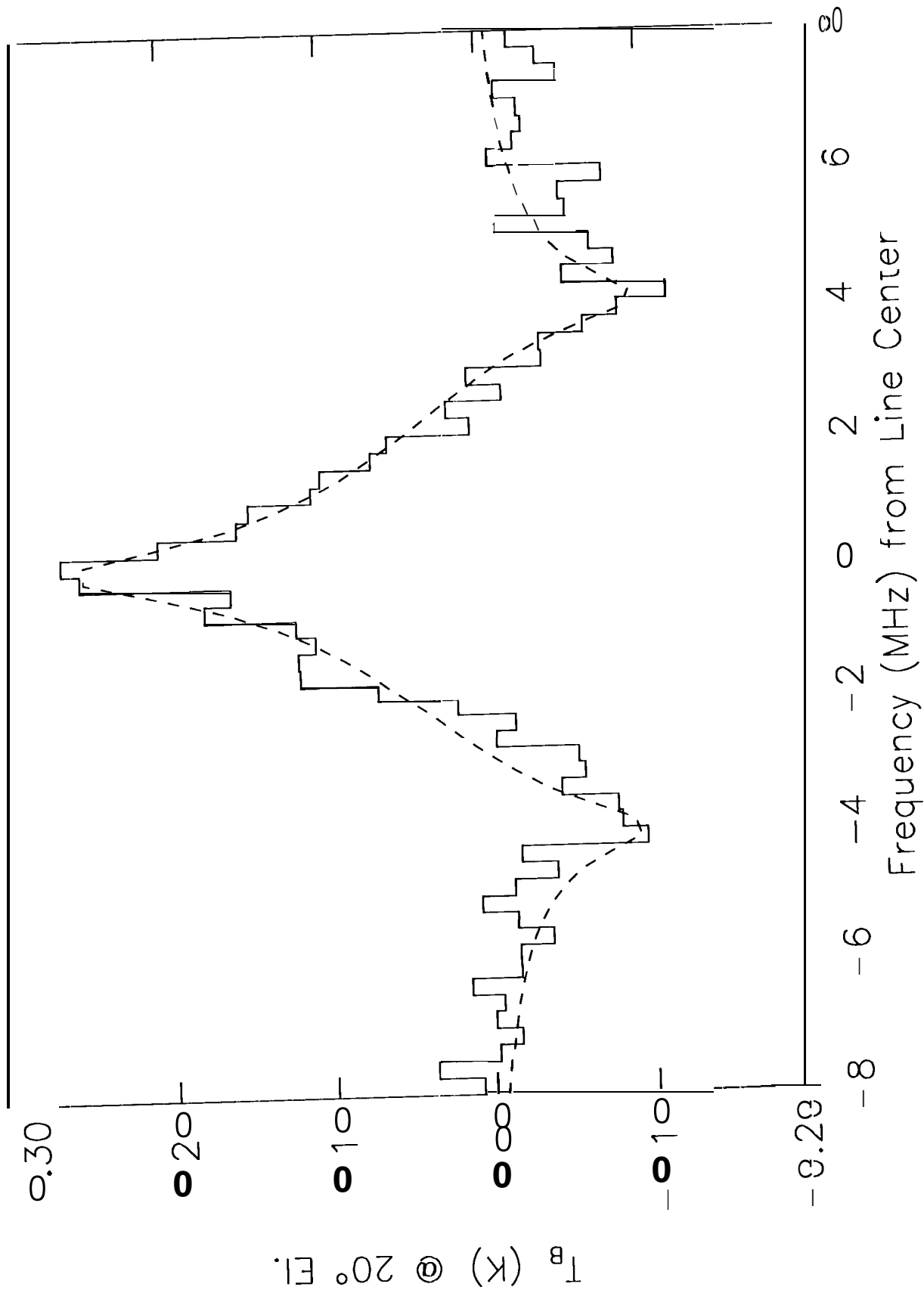


Fig 7: Observed H<sub>2</sub>O

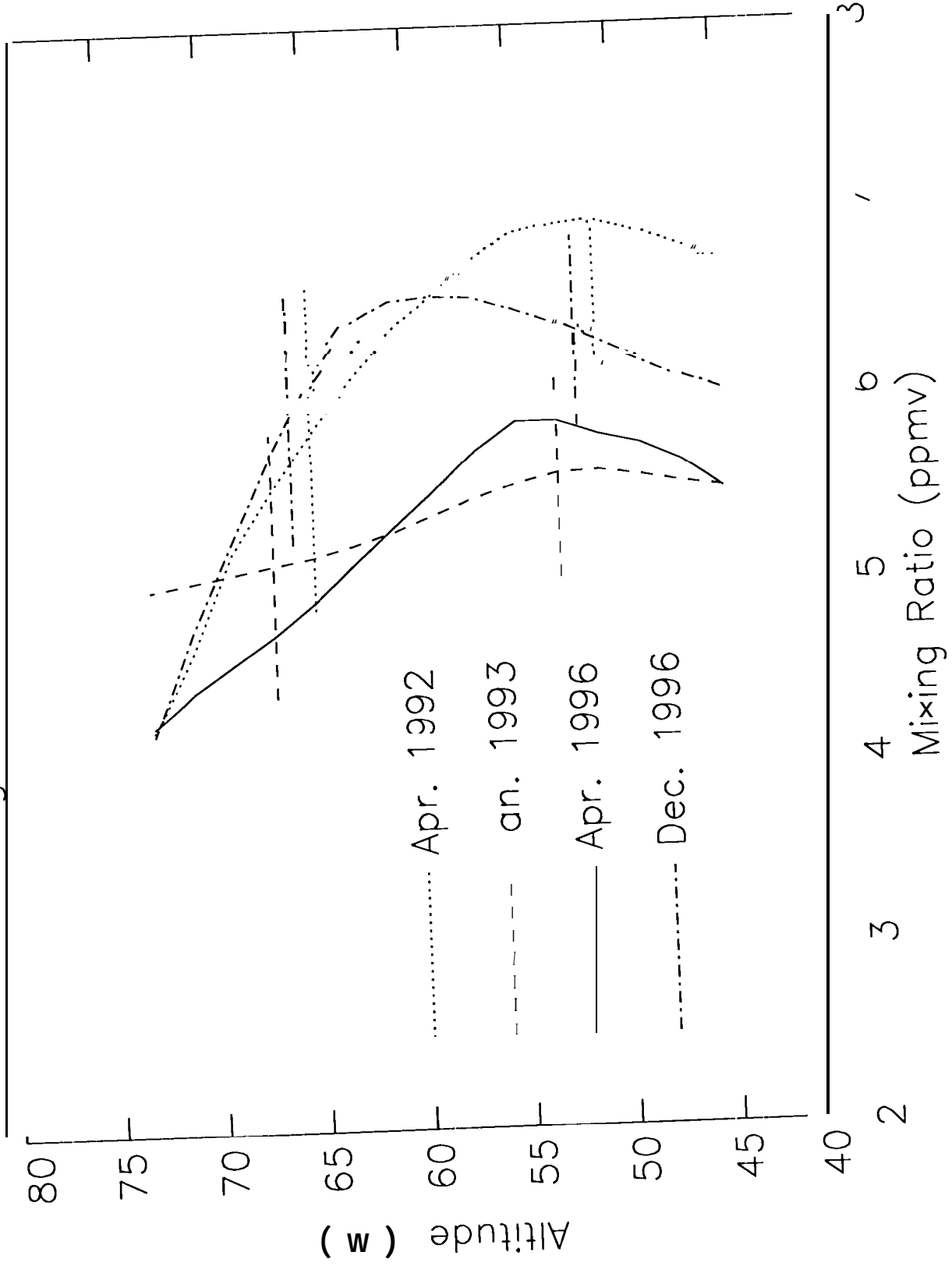


Fig.8: HO<sub>2</sub> at 70 km, 23 Jan, 1993

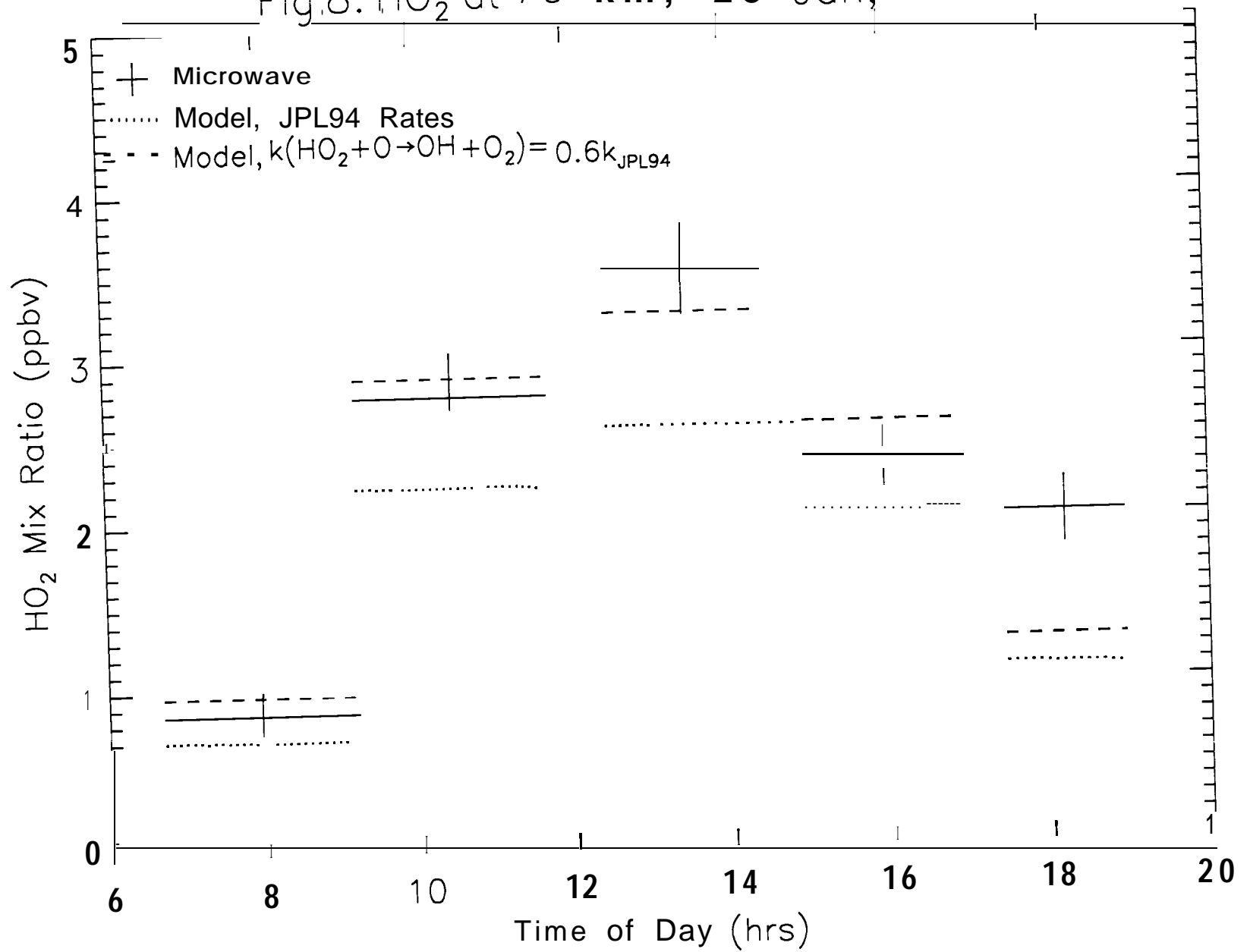


Fig. 9: HO<sub>2</sub> at 70 km, **Nov30– Dec2, 1996**

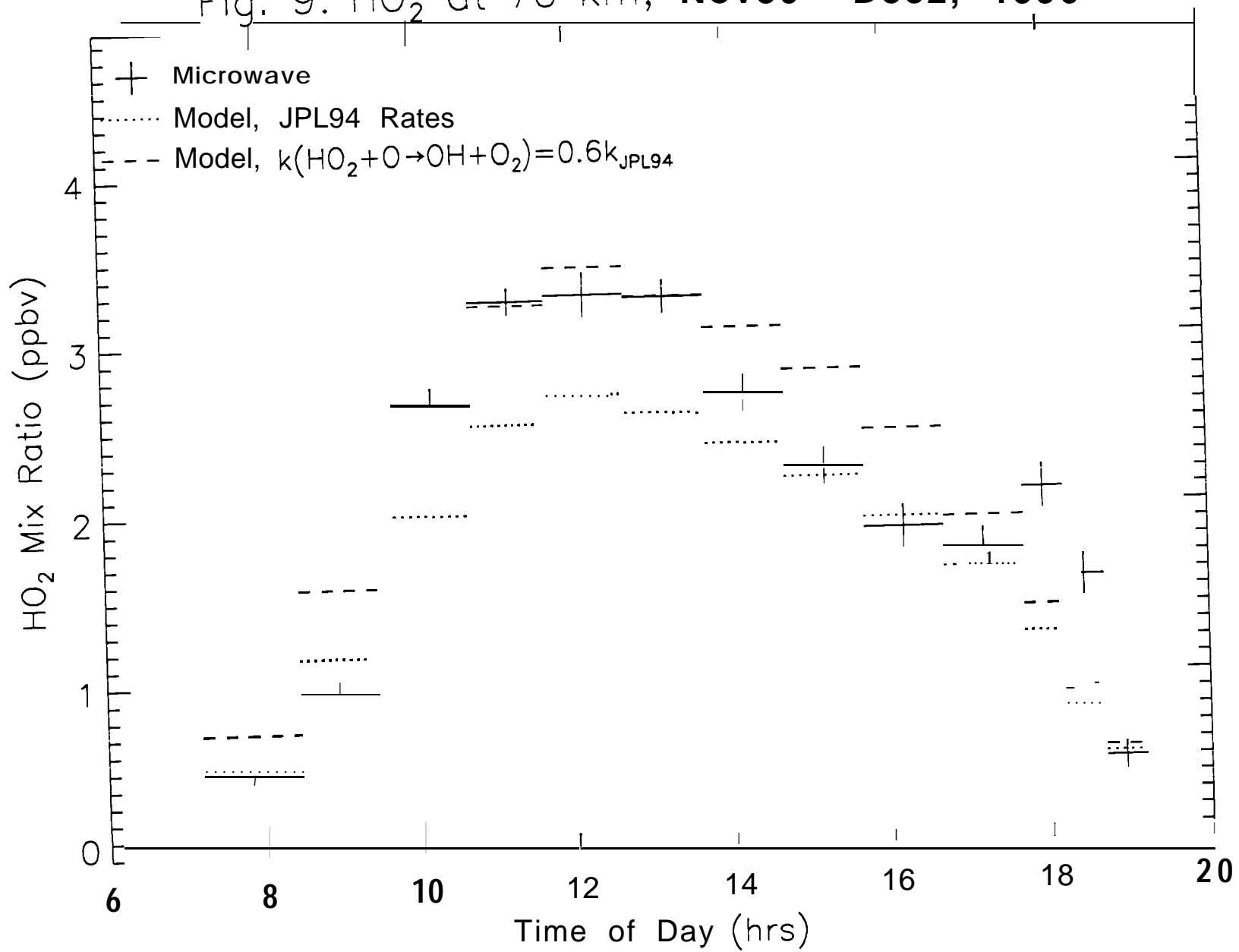
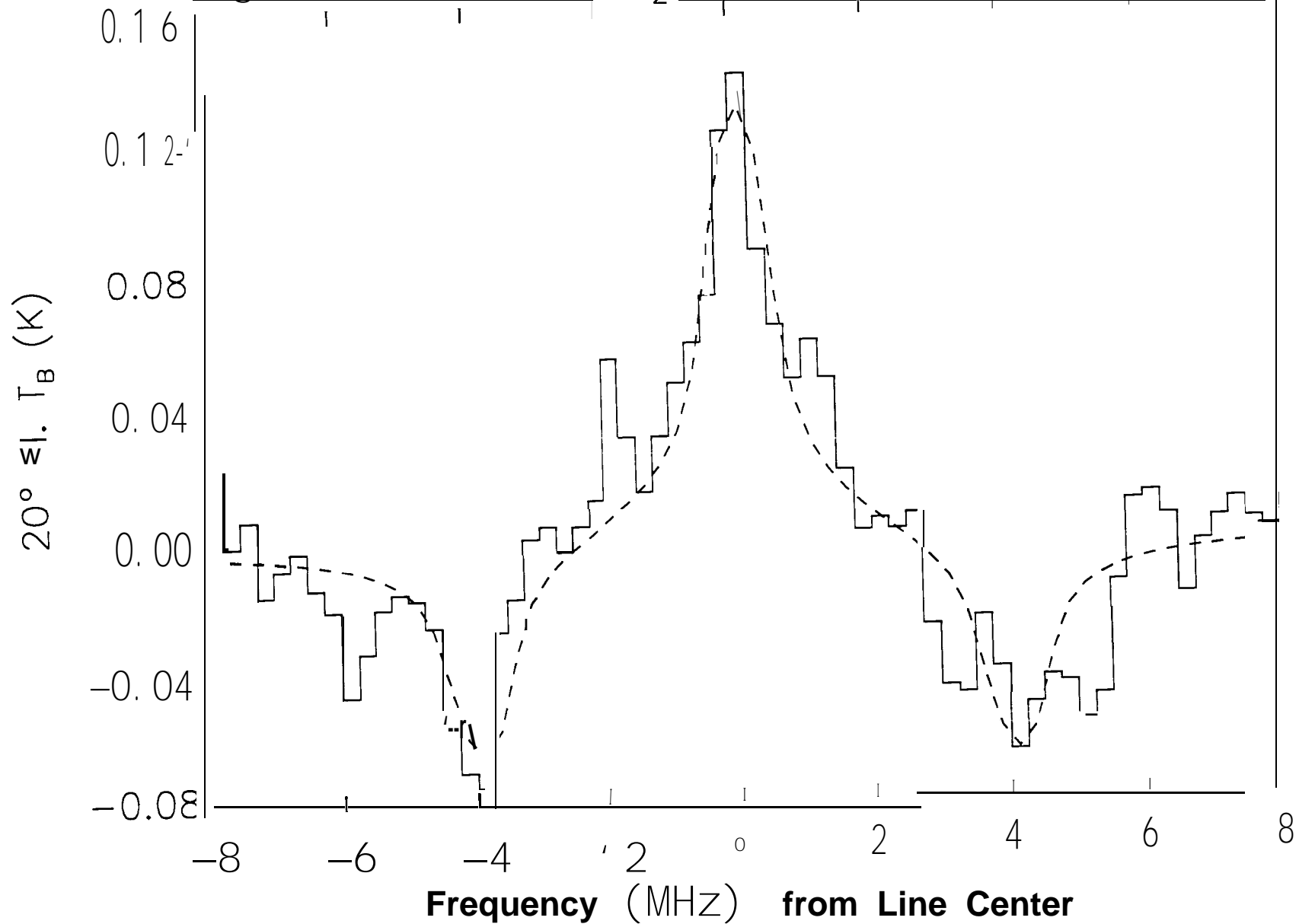


Fig 10: 260 GHz HO<sub>2</sub>, 30 Nov–2 Dec 96, 6–7 pm



**Fig. 11: Model HO<sub>2</sub> Diurnal Behavior**

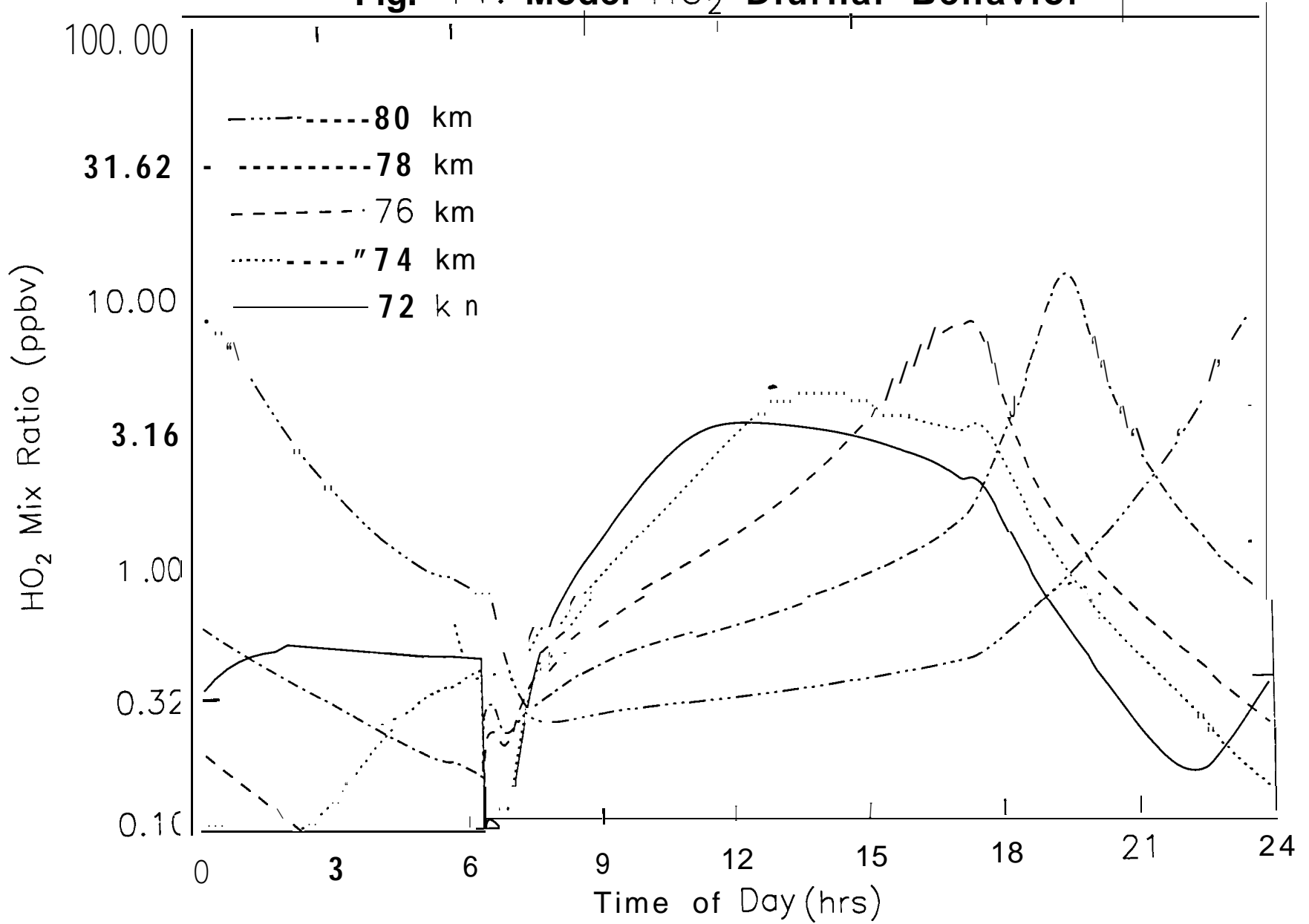


Fig. 12: 249 GHz  $O_3$ , 10 Apr92, 1:00pm

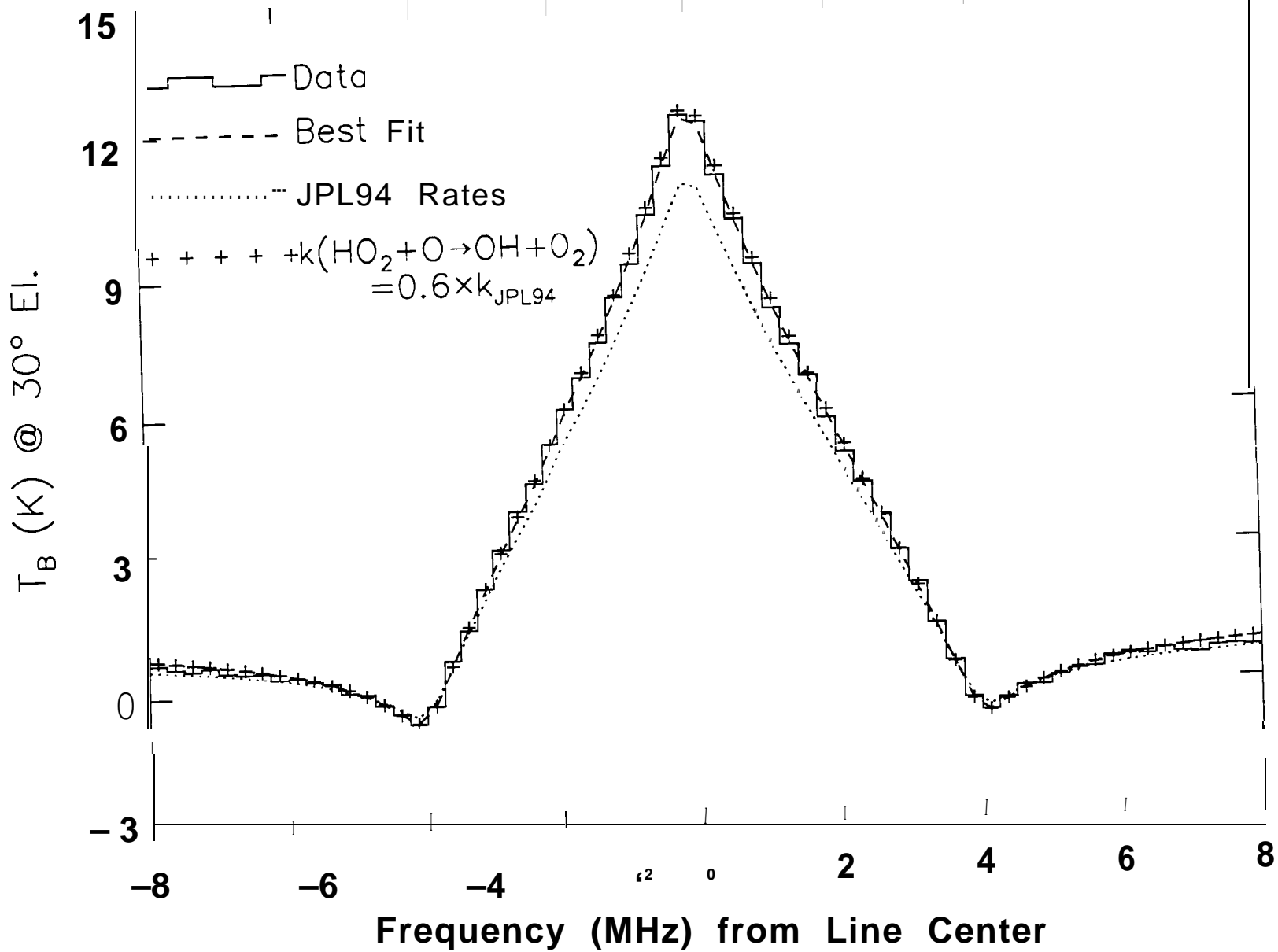


Fig. 13: 10Apr92 O<sub>3</sub> 1:∞∞m

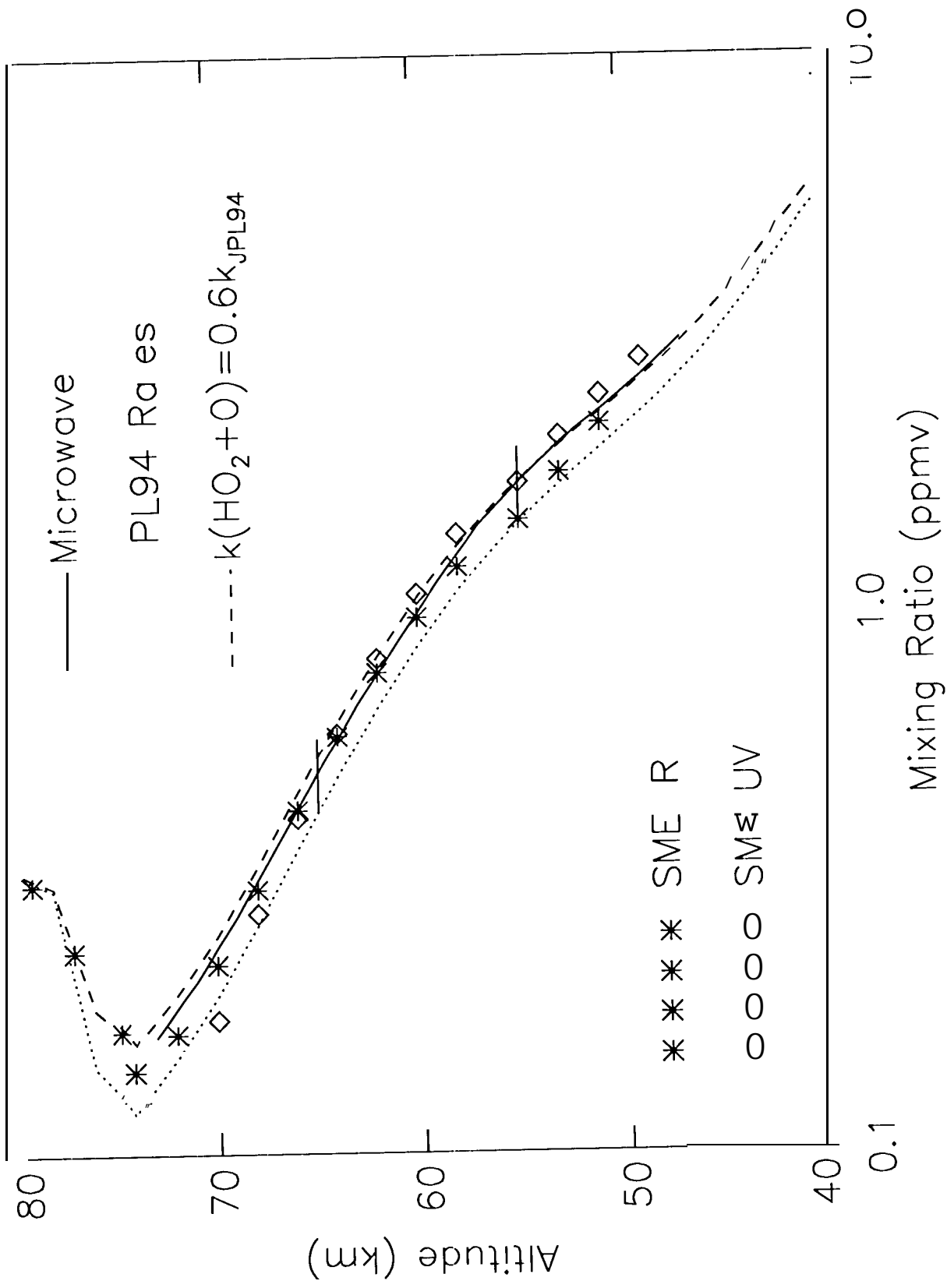


Fig 14: 23-25Jan93 O<sub>3</sub>, 52

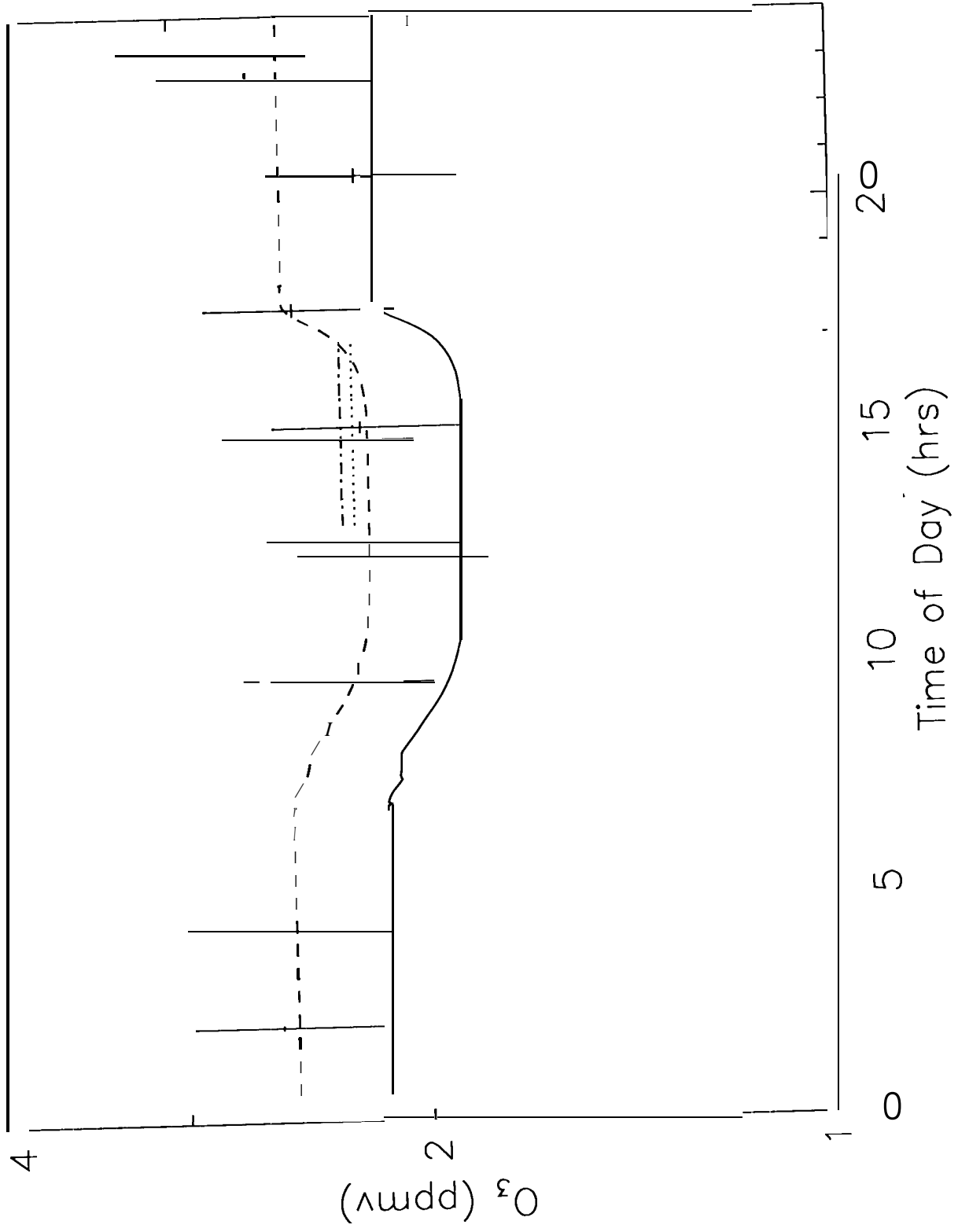


Fig 15: 23-25Jan93 O<sub>3</sub>, 60 km

